Supporting Information

Electrochemical Suzuki-Miyaura cross-coupling using peptide bolaamphiphile hydrogel-supported Pd NPs as heterogeneous electrocatalyst

Deepak K. K. Kori,[a] Tapas Ghosh,[a] Apurba K. Das*[ab]

[a]Department of Chemistry, Indian Institute of Technology Indore, Indore 453552, India

[b]Centre for Advanced Electronics (CAE), Indian Institute of Technology Indore, Indore 453552, India

E-mail: apurba.das@iiti.ac.in

Table of Contents

Materials and methods

Materials: Glutaric acid, 1-hydroxybenzotriazole (HOBt), amino acids and *N*-(3-dimethylaminopropyl)-*N'*-ethylcarbodiimide (EDC) hydrochloride were purchased from SRL chemicals, India and used without further purification. $PdCl_2$, iodobenzene and Nafion-117 solution were purchased from Sigma Aldrich Chemicals. 4-Methoxyphenylboronic acid, 3-nitrophenylboronic acid and 4-nitrophenylboronic acid (SRL chemicals), 4-chlorophenylboronic acid, 4-carboxyphenylboronic acid, pyrene-1-boronic acid (Sigma Aldrich), 4-(trifluoromethyl)phenylboronic acid, 3-thienylboronic acid and tetrabutylammonium hexafluorophosphate (TCI Chemicals), 4-(hydroxymethyl)phenylboronic acid (Alfa Aesar) were procured from various commercially available sources. Carbon paper was obtained from Global Nanotech, Mumbai, India. All solvents were analytical grade, purchased from Merck chemicals and distilled before use. Milli-Q water was used in all experiments.

Characterization methods

^{1}H and ^{13}C NMR spectra of all the precursors and final compounds were recorded on Bruker AV 500 MHz instrument using tetramethylsilane as the internal standard and DMSO-d_6 as solvent. The concentration of the compound was used in between 10-15 mmol. Mass spectra were recorded on a Bruker Daltonics LC-MS spectrometer by positive mode electron spray ionizations. FTIR spectra of the dried hydrogel and Pd@hydrogel were acquired on PerkinElmer FT-IR spectrometer. Powder X-ray diffraction (PXRD) pattern of the hydrogel and Pd@hydrogel were recorded using Rigaku SmartLab automated multipurpose X-ray diffractometer, with a wavelength of 0.54 nm (Cu Kα) a 25 ºC. X-ray photoelectron spectroscopy (XPS) measurement was carried out to determine the surface chemical state and elemental composition of the Pd@hydrogel. MP-AES analysis were carried out using Agilent 4210-MP-AES to determine the conc. of Pd loading in Pd@hydrogel. The circular dichroism (CD) spectra of the hydrogel and Pd@hydrogel were recorded using a JASCO J-815 spectropolarimeter at 25 °C. The spectra were recorded in a quartz cell of path length 1 mm within the range 300-190 nm with a data pitch of 0.1 nm. Mechanical and viscoelastic properties of the self-assembled hydrogel and Pd@hydrogel were obtained by performing rheological experiment using Anton Paar Physica MCR 301 rheometer at 25 ºC. Morphological studies were carried out by FE-SEM and HR-TEM. Field emission scanning

electron microscopic images were obtained using a Supra55 Zeiss. Further, high-resolution transmission electron microscopic images were obtained using a JEOL JEM 2100F.

Synthetic Procedure

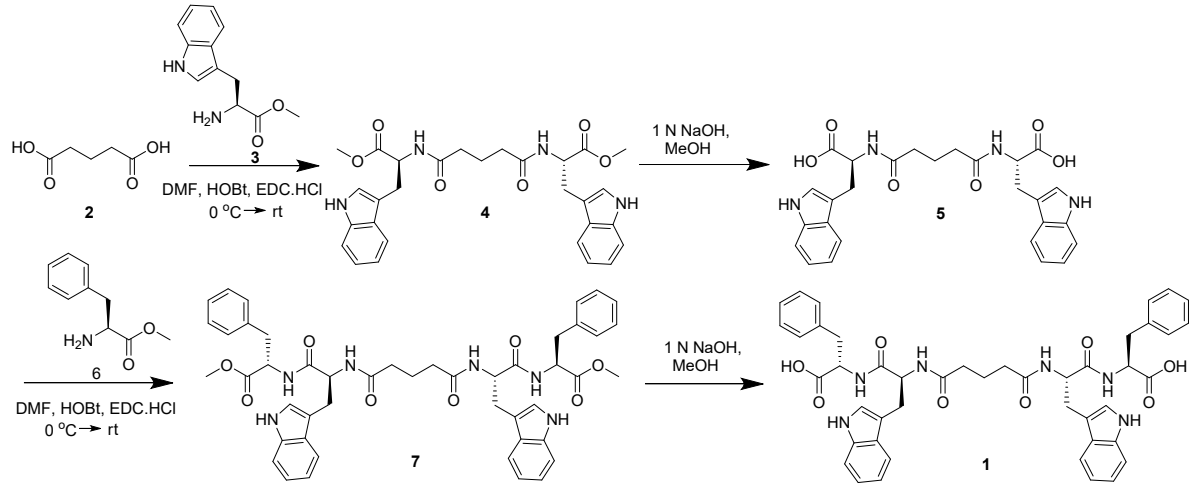

Scheme S1. Synthetic scheme for solution phase synthesis of peptide bolaamphiphile **1** (HO-F-W-GluA-W-F-OH).

Synthesis of MeO-W-GluA-W-OMe (4): 0.5 g (3.78 mmol) glutaric acid was stirred with 3 mL DMF at 0 ºC followed by addition of 1.02 g (7.56 mmol) HOBt. Soon after, 2.89 g (11.34 mmol) L-tryptophan methyl ester (**3**) was isolated from its corresponding hydrochloride salt and concentrated to add to the reaction mixture with subsequent addition of *N*-(3-dimethylaminopropyl)-*N'*-ethylcarbodiimide hydrochloride (1.59 g, 8.32 mmol). The reaction mixture was left overnight. Thereafter, reaction mixture was diluted by adding 50 mL ethyl acetate and the organic layer was washed with 1M HCl (3×50 mL), brine (2×50 mL), 1M Na_2CO_3 (3×50 mL), brine (2×50 mL) and dried over anhydride Na_2SO_4 and evaporated under vacuum to yield (**4)** as white solid. Purification was done by flash chromatography on silica gel (100-200 mesh) using ethyl acetate : hexane (9:1) as an eluent.

Yield: 94% (1.90 g, 3.57 mmol); ^{1}H NMR (500 MHz, DMSO-d_6) δ 10.86 (s, 2H, ring -NH- of Trp), 8.24 (d, J = 7.5 Hz, 2H, -NH- of Trp), 7.50 (d, J = 7.9 Hz, 2H, ring protons of Trp), 7.35 (d, J = 8.1 Hz, 2H, ring protons of Trp), 7.17-6.98 (m, 6H, ring protons of Trp), 4.55-4.48 (m, 2H, C^{α} H of Trp), 3.58 (s, 6H, -OCH_3), 3.19-3.11 (m, 2H, C^{β} Hs of Trp), 3.06-3.02 (m, 2H, C^{β} Hs of Trp), 2.15-2.02 (m, 4H, –CH_2 of GluA), 1.70-1.61 (m, 2H, –CH_2 of GluA); ^{13}C NMR (125 MHz, DMSO-d_6) δ 173.1, 172.5, 136.6, 127.5, 124.1, 121.5, 118.9, 118.5,

111.9, 110.0, 53.6, 52.2, 34.8, 27.5, 21.7; MS (ESI): *m/z* $[M+Na]^+$ calculated for $C_{29}H_{32}N_4O_6Na$ 555.2214; found: 555.2175.

Synthesis of HO-W-GluA-W-OH (5): 0.5 g (0.94 mmol) of MeO-W-GluA-W-OMe (**4**) was taken in a round bottom flask and 10 mL MeOH was added to it. In the given reaction mixture, 8 mL 1M NaOH was added and the progress of the hydrolysis was monitored using thin layer chromatography. The reaction mixture was stirred for 7 h. Once the reaction was complete, MeOH was evaporated under vacuum and 20 mL distilled water was added to it. Then, aqueous layer was washed with diethyl ether (2×30 mL). Furthermore, aqueous layer was collected and kept under ice cold condition and drop-wise 1M HCl was added to adjust the pH 2. Soon after, aqueous layer was extracted with ethyl acetate (3x50 mL) and dried over anhydride Na_2SO_4 and evaporated under vacuum to yield (**5**) as yellow solid.
Yield: 76% (0.36 g, 0.71 mmol); ^{1}H NMR (500 MHz, DMSO-d_6) δ 12.64 (s, br, 2H -COOH), 10.82 (s, 2H, ring protons of Trp), 8.08 (d, J = 8.8 Hz, 2H, -NH- of Trp), 7.63-7.49 (m, 2H, ring protons of Trp), 7.43 – 7.27 (m, 2H, , ring protons of Trp), 7.23-6.91 (m, 6H, ring protons of Trp), 4.48 (s, 2H, C^{α} H of Trp), 3.22-2.94 (m, 4H, C^{β} Hs of Trp), 2.15-1.99 (m, 4H, –CH_2 of GluA), 1.72-1.58 (m, 2H, –CH_2 of GluA); ^{13}C NMR (125 MHz, DMSO-d_6) δ 174.2, 172.4, 136.5, 127.6, 124.0, 121.4, 118.8, 118.6, 111.9, 110.4, 53.4, 34.9, 27.6, 21.9; MS (ESI): *m/z* $[M+Na]^+$ calculated for $C_{27}H_{28}N_4O_6Na$ 527.1901; found: 527.1827.

Synthesis of MeO-F-W-GluA-W-F-OMe (7): 0.24 g (0.48 mmol) HO-W-GluA-W-OH **(5)** was stirred with 3 mL DMF at 0 °C followed by addition of 0.13 g (0.96 mmol) HOBt. Soon after, 0.31 g (1.44 mmol) L-phenylalanine methyl ester **(6)** was isolated from its corresponding hydrochloride salt and concentrated to add to the reaction mixture with subsequent addition of *N*-(3-Dimethylaminopropyl)-*N'*-ethylcarbodiimide hydrochloride (0.20 g, 1.06 mmol). The reaction mixture was left overnight. Thereafter, reaction mixture was diluted by adding 50 mL ethyl acetate and the organic layer was washed with 1M HCl (3×50 mL), brine (2×50 mL), 1M Na_2CO_3 (3×50 mL), brine (2×50 mL) and dried over anhydride Na_2SO_4 and evaporated under vacuum to yield **(7)** as white solid. Purification was done by flash chromatography on silica gel (100-200 mesh) using ethyl acetate: hexane (9:1) as an eluent.
Yield: 89% (0.35 g, 0.42 mmol); ^{1}H NMR (500 MHz, DMSO-d_6) δ 10.83 (s, 2H, ring -NH- of Trp), 8.92 (d, J = 7.0 Hz, 2H, -NH- of Phe), 8.37 (d, J = 8.2 Hz, 2H, -NH- of Trp), 7.75 (d,

J = 7.9 Hz, 2H, ring protons of Trp), 7.32-7.28 (m, 4H, ring protons of Phe), 7.27 (s, 6H, ring protons of Phe), 7.21 (d, *J* = 6.7 Hz, 2H, ring protons of Trp), 7.18 (d, *J* = 2.4 Hz, 2H, ring protons of Trp), 7.06 (t, *J* = 7.7 Hz, 2H, ring protons of Trp), 6.98 (t, *J* = 7.4 Hz, 2H, ring protons of Trp), 4.60-4.53 (m, 4H, C^{α} H of Trp and Phe), 3.53 (s, 6H, -OCH_3), 3.13 – 3.05 (m, 6H, C^{β} Hs of Trp and Phe), 2.88 – 2.83 (m, 2H, C^{β} Hs of Phe), 1.89-1.75 (m, 4H, –CH_2 of GluA), 1.62-1.54 (m, 2H, –CH_2 of GluA); ^{13}C NMR (125 MHz, DMSO-d_6) δ 174.1, 172.2, 137.5, 136.6, 129.6, 128.8, 127.6, 127.1, 124.5, 121.3, 119.2, 118.6, 111.7, 110.5, 54.6, 53.8, 52.3, 37.0, 34.1, 28.2, 22.3; MS (ESI): *m/z* $[M+Na]^+$ calculated for $C_{47}H_{50}N_6O_8Na$ 849.3582; found: 849.3656.

Synthesis of HO-F-W-GluA-W-F-OH (1): 0.35 g (0.42 mmol) of MeO-F-W-GluA-W-F-OMe **(7)** was taken in a round bottom flask and 8 mL MeOH was added to it. In the reaction mixture, 6 mL of 1M NaOH was added and the progress of the hydrolysis was monitored using thin layer chromatography. The reaction mixture was stirred for 7 h. Once the reaction was completed, MeOH was evaporated under vacuum and 20 mL distilled water was added to it. Then, aqueous layer was washed with diethyl ether (2×30 mL). Furthermore, aqueous layer was collected and kept under ice cold condition and drop wise 1M HCl was added to adjust the pH 2. Soon after, aqueous layer was extracted with ethyl acetate (3×50 mL) and dried over anhydride Na_2SO_4 and evaporated under vacuum to yield (**1**) as white solid.
Yield: 73% (0.25 g, 0.31 mmol); ^{1}H NMR (500 MHz, DMSO-d_6) δ 10.81 (d, *J* = 2.2 Hz, 2H, ring -NH- of Trp), 8.72 (d, *J* = 7.6 Hz, 2H, -NH- of Phe), 8.35 (d, *J* = 8.3 Hz, 2H, -NH- of Trp), 7.77 (d, *J* = 7.9 Hz, 2H, ring protons of Trp), 7.33-7.25 (m, 10H, ring protons of Phe), 7.24 – 7.20 (m, 4H, ring protons of Trp), 7.07 (t, *J* = 7.6 Hz, 2H, ring protons of Trp), 7.00 (t, *J* = 7.4 Hz, 2H, ring protons of Trp), 4.66-4.52 (m, 4H, C^{α} H of Trp and Phe), 3.16-3.12 (m, 4H, C^{β} Hs of Trp), 3.08-3.03 (m, 2H, C^{β} Hs of Phe), 2.92-2.87 (m, 2H, C^{β} Hs of Phe), 1.84 (t, *J* = 7.0 Hz, 4H, –CH_2 of GluA), 1.62-1.53 (m, 2H, –CH_2 of GluA); ^{13}C NMR (125 MHz, DMSO-d_6) δ 173.9, 173.2, 172.4, 137.9, 136.6, 129.6, 128.7, 127.6, 126.9, 124.6, 121.3, 119.2, 118.6, 111.8, 110.5, 54.3, 53.9, 37.1, 34.2, 28.3, 22.3; MS (ESI): *m/z* $[M+Na]^+$ calculated for $C_{45}H_{46}N_6O_8Na$ 821.3269; found: 821.3278.

Morphological study of Hydrogel and Pd@hydrogel

Transmission electron microscopy (TEM) measurements were carried out to investigate the morphology of self-assembled hydrogel and Pd@hydrogel. TEM images were acquired by using JEOL JEM 2100F with an accelerating voltage of 300 kV. In the experiment, 50 µL of

hydrogel (25 mM) was added in the micro centrifuge tube containing 450 µL DI water. Then, 20 µL of diluted solution was pipetted onto a carbon-coated copper grid (300 mesh) and allowed to dry by slow evaporation in the air and separately under reduced pressure at room temperature. Phosphotungstic acid (2% w/v) was used as a negative agent for hydrogel. Field emission Gun-scanning electron microscopic experiments were conducted by using Carl Zeiss scanning electron microscope (FE-SEM Supra 55 Zeiss). A portion of 100 µL of hydrogel (25 mM) was diluted with 500 µL DI water and then 20 µL was pipetted onto a glass coverslip. Further, the glass coverslips were allowed to dry in air and then under vacuum overnight. The glass coverslips were coated with copper and the images were recorded with an operating voltage of 5 kV.

Rheological Study

Rheological analyses were performed to evaluate the mechanical properties of hydrogels by Anton Paar Physica MCR 301 Rheometer with a parallel plate-geometry (diameter: 25 mm, trugap: 0.5 mm). Hydrogel and Pd@hydrogel were transferred onto a rheometer plate by using a micro spatula and kept hydrated by using a solvent trap. The dynamic strain sweep measurements were conducted to determine the region of deformation in which linear viscoelasticity is valid. Linear viscoelastic regime (LVR) was used to determine the exact strain of self-assembled hydrogel and Pd@hydrogel at a constant frequency of 10 rad s^{-1}. The mechanical strength of hydrogel and Pd@hydrogel were evaluated by performing dynamic frequency sweep measurements in the frequency range of 0.5-100 rad s^{-1} with a constant strain value of 1%.

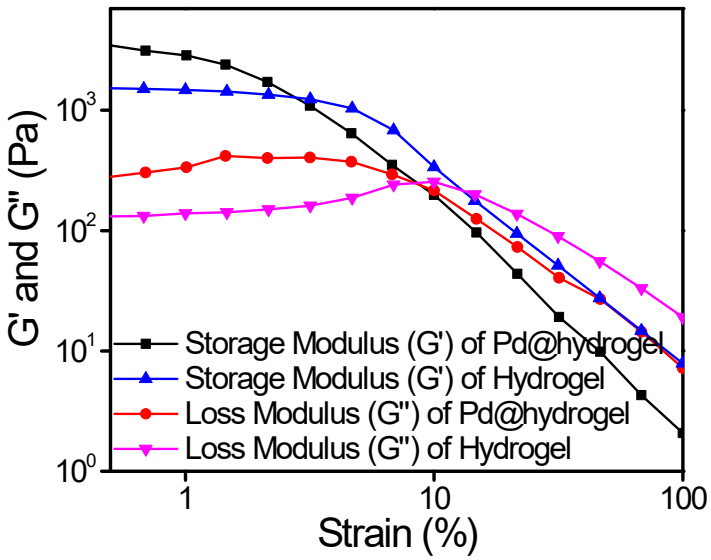

Fig. S1. Amplitude strain sweep experiment (at constant frequency 1 rad s^{-1}) of hydrogel and Pd@hydrogel at pH 7.4.

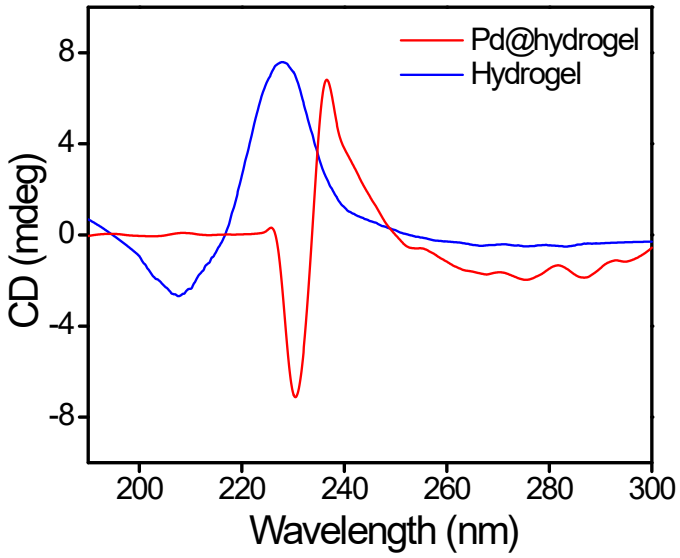

Fig. S2. CD spectra of Pd@hydrogel and peptide bolaamphiphile based hydrogel.

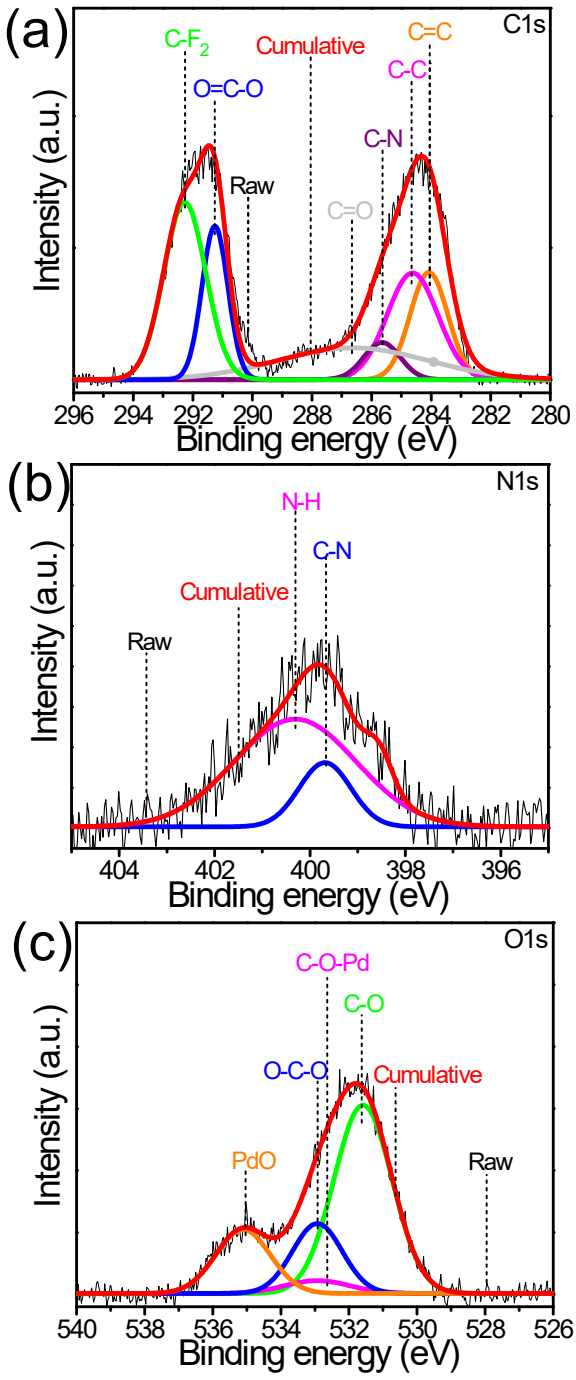

Fig. S3. Pd@hydrogel high-resolution XPS spectrum of (a) C 1s, (b) N 1s and (c) O 1s.

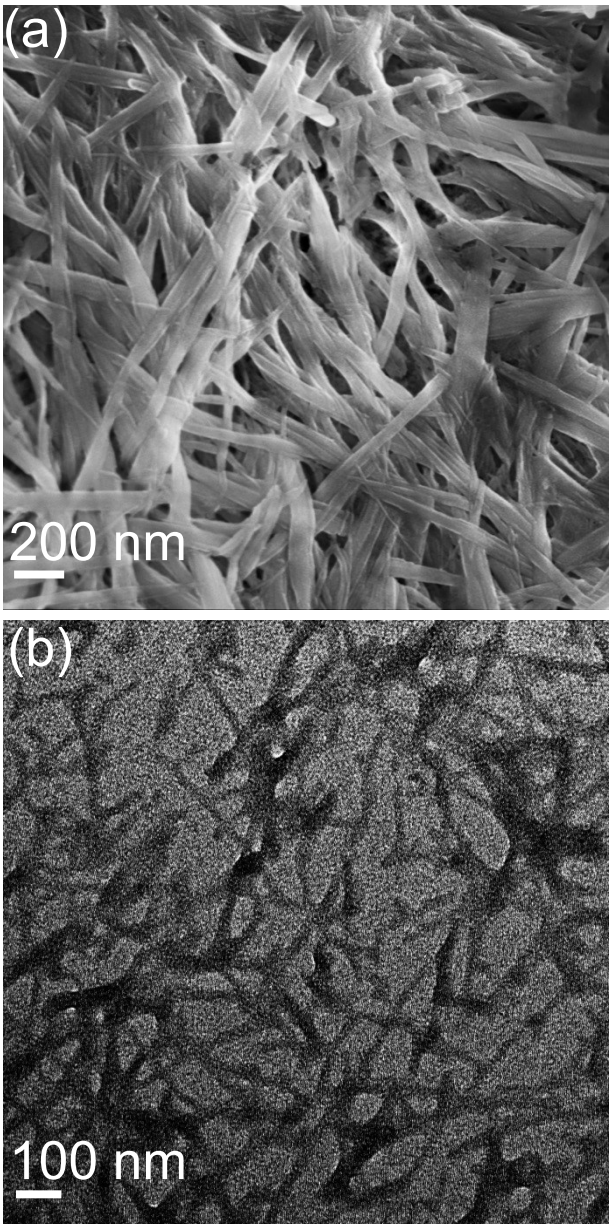

Fig. S4. (a) FE-SEM image and (b) TEM image of peptide bolaamphiphile based hydrogel.

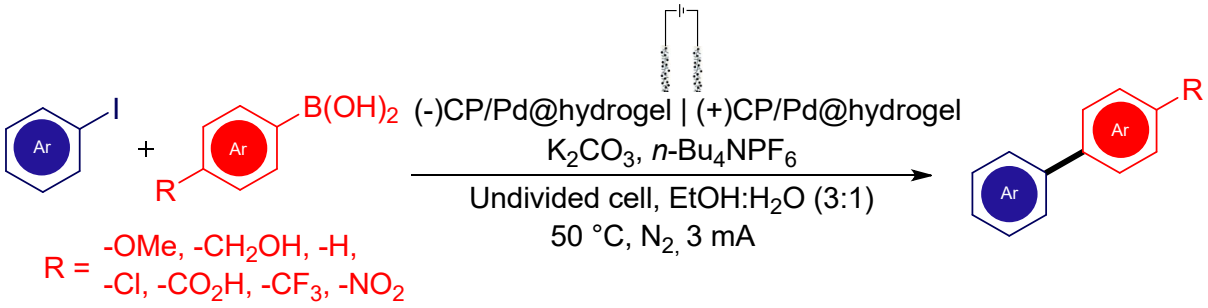

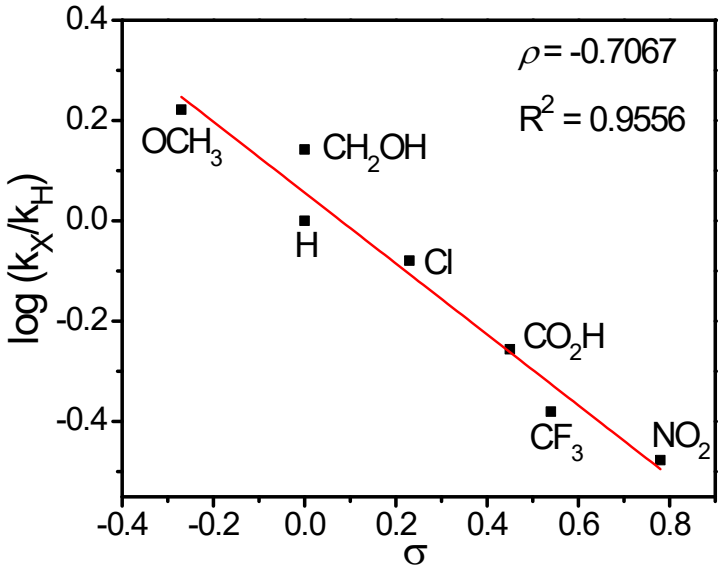

Fig. S5. Hammett plot for the electrochemical Suzuki-Miyaura cross-coupling reactions of *para*-substituted arylboronic acids.

Electrochemical procedure for Cyclic voltammetry (CV)

Cyclic voltammetry measurements were performed in an Autolab potentiostat (PGSTST309) electrochemical workstation using three-electrode setups under N_2 at room temperature (25° C). Platinum wire, Ag/AgCl and glassy carbon disk were served as a reference, counter and working electrodes, respectively. 30 mL solvent containing CH_3CN, *n*-Bu_4NPF_6 (0.05 M), were immersed in an undivided electrochemical cell. Redox potentials were reported against Ag/AgCl reference electrode. The scan rate was 200 mV/s, ranging from 3 V to -3 V.

Procedures for CVs of blank, iodobenzene, K_2CO_3 and 4-methoxyphenylboronic acid

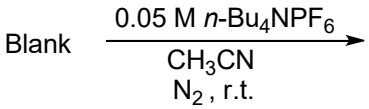

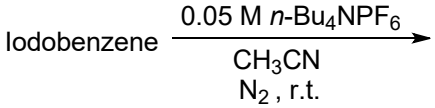

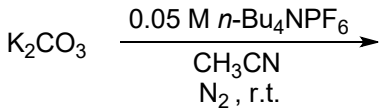

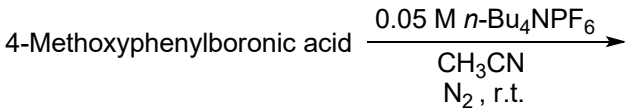

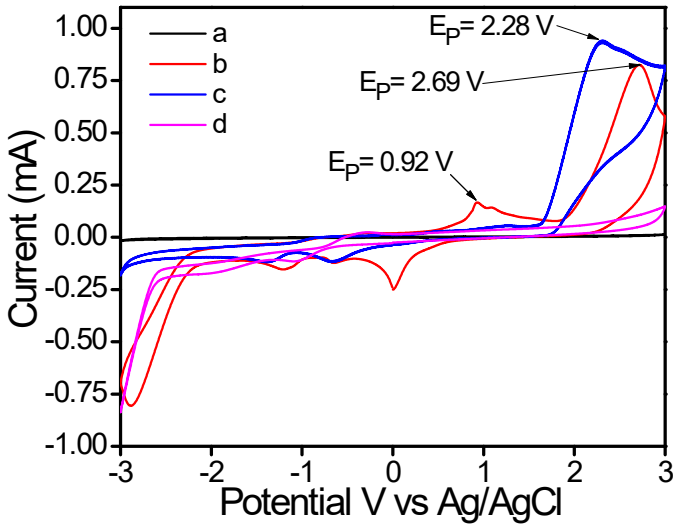

Fig. S6. Cyclic Voltammogram for (a) Blank glassy carbon. (b) 0.65 mM iodobenzene. (c) 0.82 mM 4-methoxyphenylboronic acid. (d) 1.64 mM K_2CO_3 in CH_3CN at 200 mV s^{-1}.

A dry undivided electrochemical cell vial (80 mL) equipped with a rubber septum and a stir bar, was charged with 4-methoxyphenylboronic acid (0.82 mM), aryl iodide (0.65 mM), K_2CO_3 (1.64 mM), *n*-Bu_4NPF_6 (0.05 M) and 30 mL CH_3CN. The undivided cell was equipped with platinum wire, Ag/AgCl and glassy carbon disk electrode (diameter 3.00 mm) as the counter, reference and working electrode, respectively.

The scan rate was 200 mV/s, ranging from 3 to -3 V. All the potentials were referenced against Ag/AgCl reference electrode.

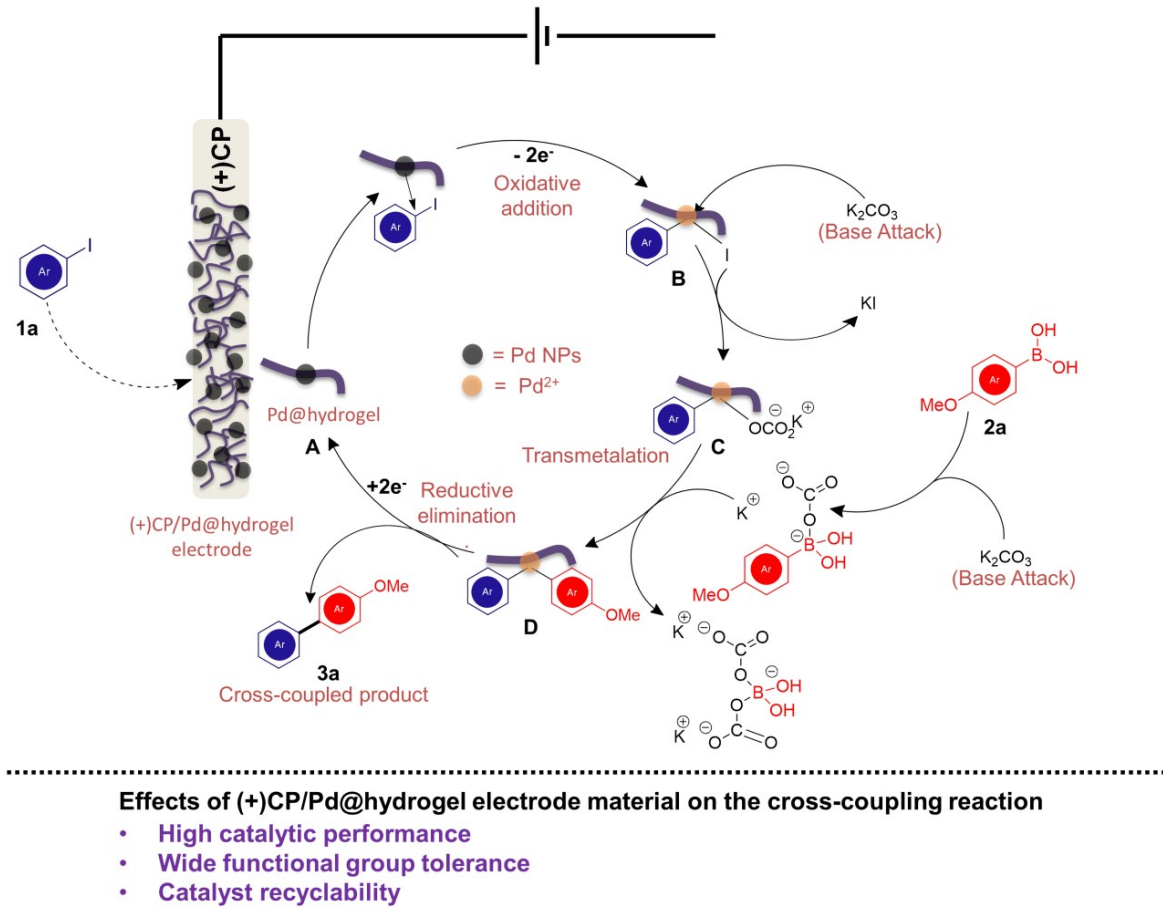

Scheme S2. Schematic representation of plausible reaction mechanism for the electrochemical Suzuki-Miyaura cross-coupling reaction on the nanofibrillar Pd@hydrogel deposited on the carbon paper (CP) electrode.

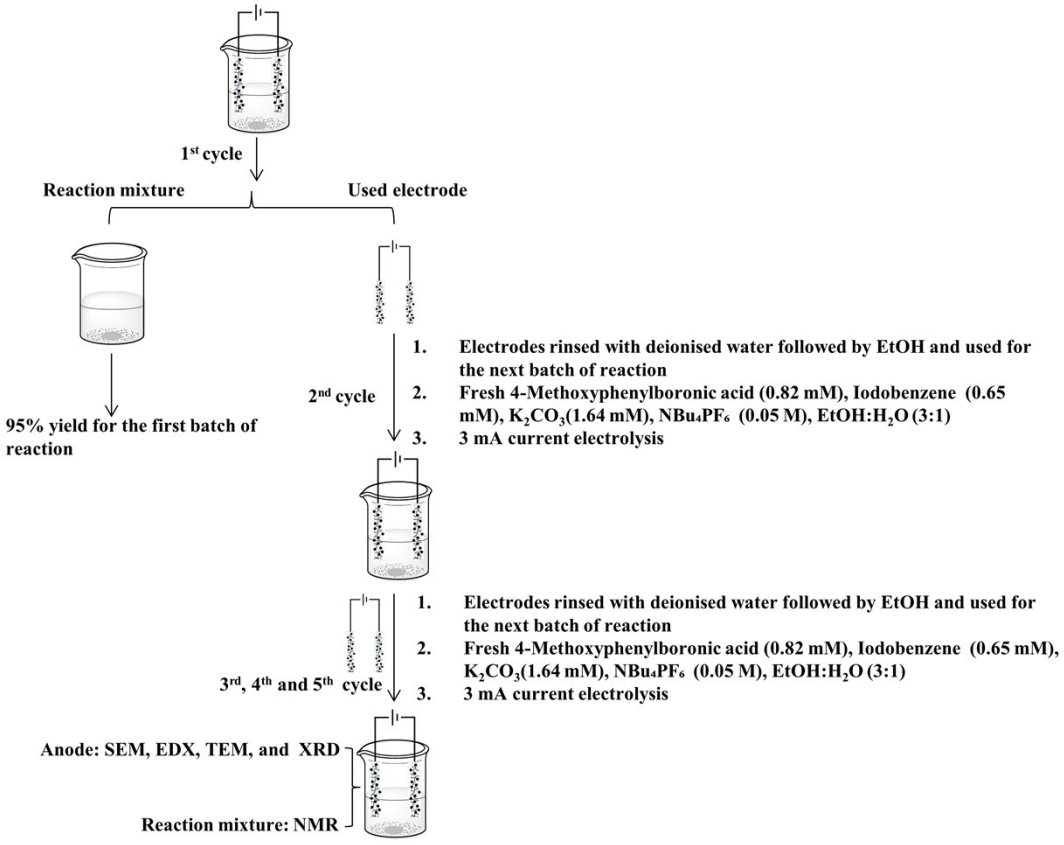

Scheme S3. Schematic representation for the recyclability test of Pd@hydrogel toward electrochemical Suzuki-Miyaura cross-coupling reaction.

^{1}H and ^{13}C NMR of the reaction mixture

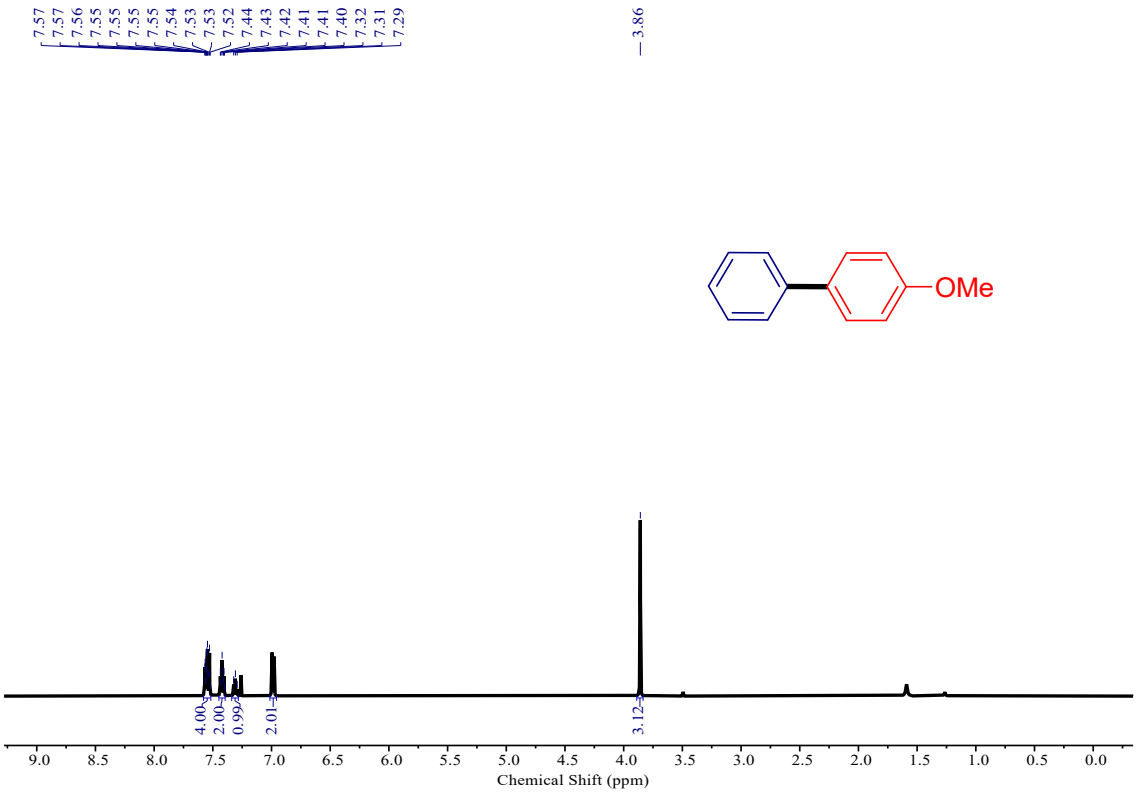

Fig. S7. ^{1}H NMR (500 MHz, $CDCl_3$) of 4-methoxy-1,1'-biphenyl isolated after fifth catalytic cycle.

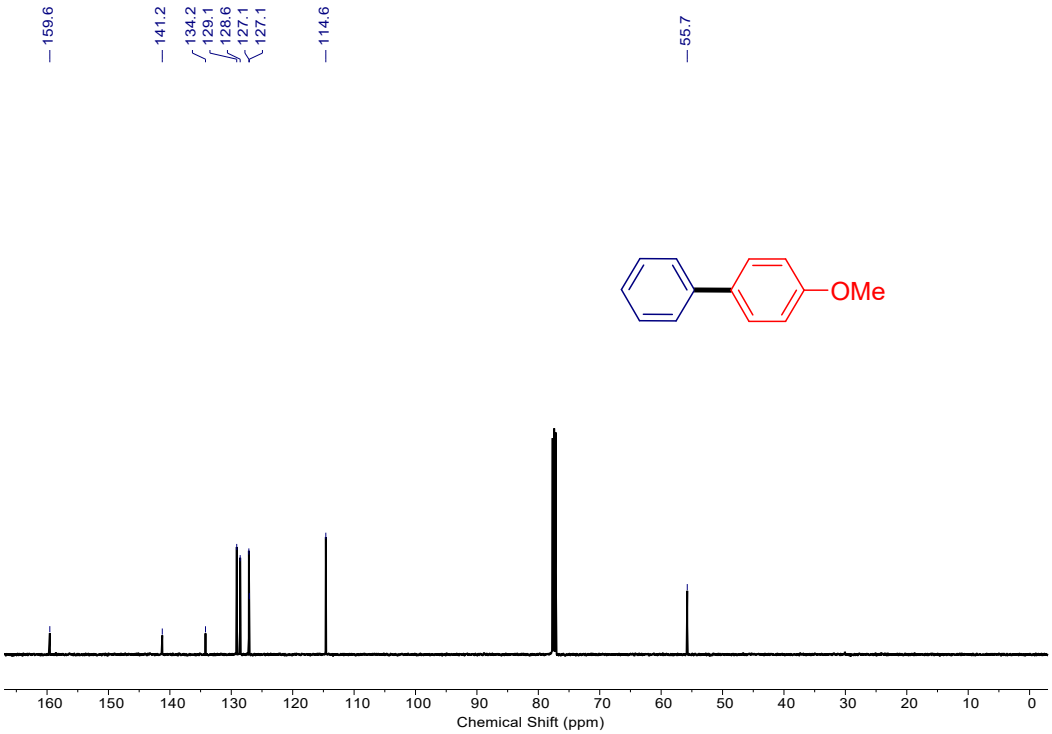

Fig. S8. ^{13}C NMR (125 MHz, $CDCl_3$) of 4-methoxy-1,1'-biphenyl isolated after fifth catalytic cycle.

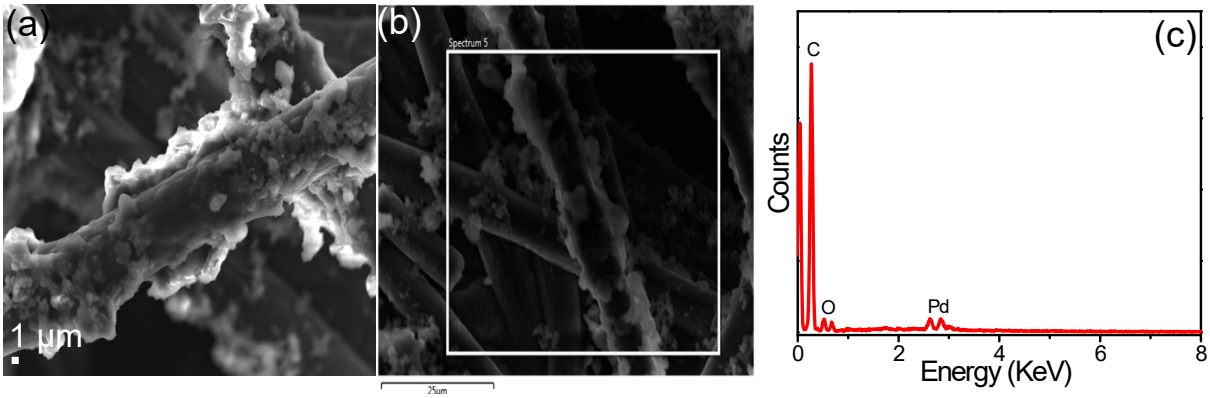

Fig. S9. FE-SEM micrographs of (a) Pd@hydrogel before the catalytic cycle. (b) and (c) SEM-EDX spectra exhibiting the chemical composition and element distribution of elements.

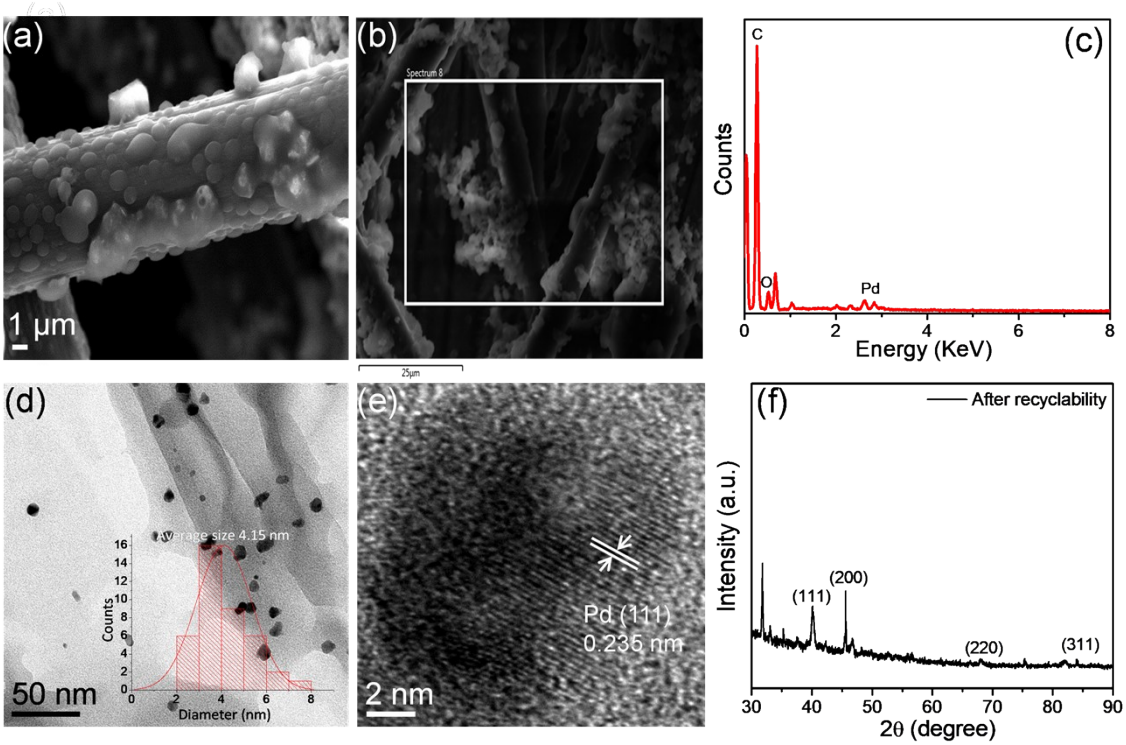

Fig. S10. (a) FE-SEM micrographs, (b) and (c) SEM-EDX spectra exhibiting the chemical composition and element distribution of elements. (d) HR-TEM image of Pd NPs entrapped in Pd@hydrogel (inset shows the histogram indicating the size of Pd NPs obtained from HR-TEM image). (e) Displays the lattice fringes of Pd. (f) Powder XRD patterns of Pd@hydrogel after the fifth catalytic cycle.

Table S1. Content of Pd in various Pd@hydrogel as determined by MP-AES

Catalyst	Pd loading (mmol)	Pd wt%
Pd@hydrogel-1	0.006	3.40
Pd@hydrogel-2	0.011	5.74
Pd@hydrogel-3	0.013	6.80

Table S2. TON of different Pd@hydrogel calculated for the electrochemical Suzuki-Miyaura cross-coupling reaction between iodobenzene **1a** and 4-methoxyphenylboronic acid **2a**

Catalyst	TON
Pd@hydrogel-1	82
Pd@hydrogel-2	71
Pd@hydrogel-3	61

Table S3. Comparative catalytic activity of Pd@hydrogel with other reported Pd based nanomaterials for the Suzuki-Miyaura cross-coupling reactions

Catalyst	X	R	Solvent	Time (h)	Yield %	Temp.	Method	References
ERGO-Pd	I	H	Ethanol	1	95	Reflux	Non-electrochemical	72
Pd/Nf -G	I	H	Ethanol / H_2O	1	96	80 °C	Non-electrochemical	73
Poly-3-graphite electrode	Br	H	Toluene/ MeOH (3:1)	12		85 °C	Non-electrochemical	74
PdNP-PG	I	H	H_2O	-	98	90 °C	Non-electrochemical	75
PVP-$PdNPs^{8nm}$	I	H	Ethanol / H_2O (1:3)	2	94	90 °C	Non-electrochemical	76
C-felt/poly-1aab	I	H	Toluene	24	30	65 °C	Non-electrochemical	77
Pd@hydrogel -2	**I**	**OMe**	**Ethanol / H_2O (3:1)**	**0.5**	**95**	**50** °C	**Electrochemical**	**This work**

Table S4. Logarithmic values of relative rate constants against standard σ values

Substrate	$Log(k_X/k_H)$	σ
OCH_3	0.2216	-0.27
CH_2OH	0.14238	0
Cl	-0.0792	0.23
CO_2H	-0.2559	0.45
CF_3	-0.3803	0.54
NO_2	-0.4771	0.78
H	0.00	0.00
ρ = -0.7067		

Characterization data of the products

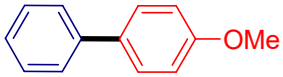

3a

^{1}H NMR (500 MHz, $CDCl_3$) δ 7.51-7.43 (m, 4H), 7.34 (t, J = 7.6 Hz, 2H), 7.27-7.19 (m, 1H), 6.91 (d, J = 8.5 Hz, 2H), 3.78 (s, 3H); ^{13}C NMR (125 MHz, $CDCl_3$) δ 159.2, 140.8, 133.8, 128.7, 128.2, 126.8, 126.7, 114.2, 55.4.

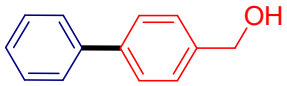

3b

^{1}H NMR (500 MHz, $CDCl_3$) δ 7.63-7.54 (m, 4H), 7.47-7.40 (m, 4H), 7.39-7.31 (m, 1H), 4.75 (s, 2H) 1.67 (s, 1H); ^{13}C NMR (125 MHz, $CDCl_3$) δ 140.8, 140.7, 139.9, 128.8, 127.5, 127.4, 127.3, 127.1, 65.2.

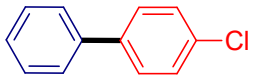

3c

^{1}H NMR (500 MHz, $CDCl_3$) δ 7.57 (d, J = 7.4 Hz, 2H), 7.54-7.51 (m, 2H), 7.48-7.40 (m, 4H), 7.37 (m, 1H); ^{13}C NMR (125 MHz, $CDCl_3$) δ 140.0, 139.7, 137.5, 133.4, 130.3, 128.9, 128.9, 128.4, 127.6, 127.0.

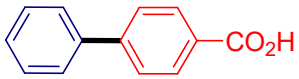

3d

^{1}H NMR (500 MHz, DMSO-d_6) δ 13.05 (s, 1H), 8.16-8.00 (m, 2H), 7.85-7.66 (m, 4H), 7.57-7.35 (m, 3H); ^{13}C NMR (125 MHz, DMSO-d_6) δ 167.7, 144.8, 139.5, 130.5, 130.2, 129.5, 128.7, 127.4, 127.2.

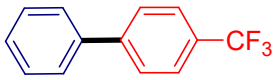

3e

^{1}H NMR (500 MHz, $CDCl_3$) δ 7.75-7.71 (m, 4H), 7.65-7.61 (m, 2H), 7.53-7.48 (m, 2H), 7.47-7.41 (m, 1H); ^{13}C NMR (125 MHz, $CDCl_3$) δ 144.8, 139.8, 129.0, 128.2, 127.4, 127.3, 125.8, 125.7, 125.7.

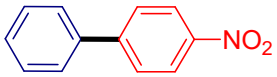

3f

^{1}H NMR (500 MHz, $CDCl_3$) δ 8.28-8.19 (m, 2H), 7.70-7.64 (m, 2H), 7.58-7.52 (m, 2H), 7.47-7.41 (m, 2H), 7.40-7.36 (m, 1H); ^{13}C NMR (125 MHz, $CDCl_3$) δ 147.7, 138.8, 129.2, 128.9, 127.8, 127.4, 124.1.

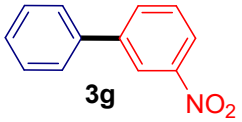

3g

^{1}H NMR (500 MHz, $CDCl_3$) δ 8.46 (t, J = 2.0 Hz, 1H), 8.22-8.18 (m, 1H), 7.93-7.90 (m, 1H), 7.64-7.59 (m, 3H), 7.52-7.48 (m, 2H), 7.46-7.42 (m, 1H); ^{13}C NMR (125 MHz, $CDCl_3$) δ 148.8, 142.9, 138.7, 133.1, 129.7, 129.2, 128.6, 127.2, 122.1, 122.0.

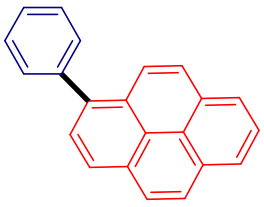

3h

^{1}H NMR (500 MHz, $CDCl_3$) δ 8.25-8.17 (m, 4H), 8.10 (d, J = 8.9 Hz, 2H), 8.05-7.99 (m, 3H), 7.68-7.63 (m, 2H), 7.61-7.55 (m, 2H), 7.53-7.46 (m, 1H); ^{13}C NMR (125 MHz, $CDCl_3$) δ 141.2, 137.8, 131.5, 131.2, 131.0, 130.6, 130.6, 128.5, 128.4, 127.6, 127.5, 127.4, 127.4, 127.3, 126.0, 125.9, 125.3, 125.1, 125.0, 125.0, 124.9, 124.8, 124.7.

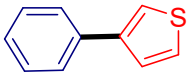

3i

^{1}H NMR (500 MHz, $CDCl_3$) δ 7.64 (d, *J* = 7.6 Hz, 2H), 7.49 (t, *J* = 2.1 Hz, 1H), 7.46-7.39 (m, 4H), 7.33 (t, *J* = 7.4 Hz, 1H); ^{13}C NMR (125 MHz, $CDCl_3$) δ 142.5, 136.0, 128.9, 127.3, 126.6, 126.5, 126.3, 120.4.

^{1}H NMR and ^{13}C NMR data of the products

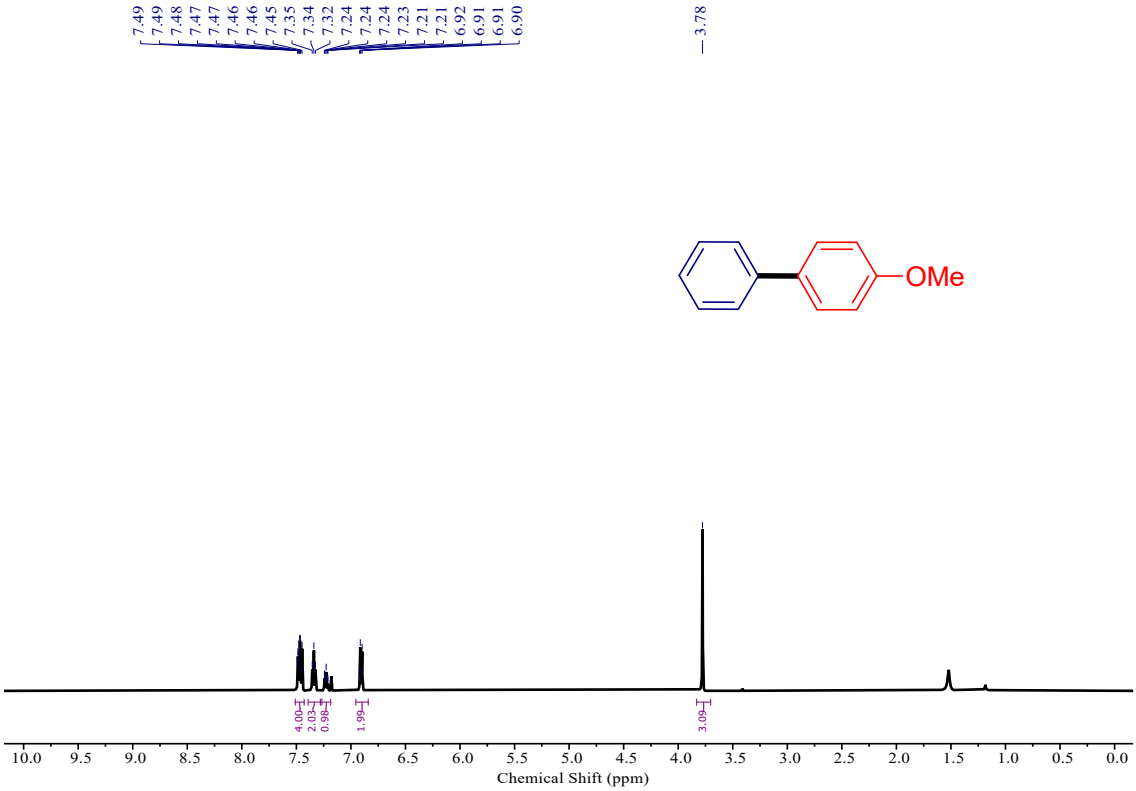

Fig. S11. ^{1}H NMR (500 MHz, $CDCl_3$) spectrum of 4-methoxy-1,1'-biphenyl **(3a)**.

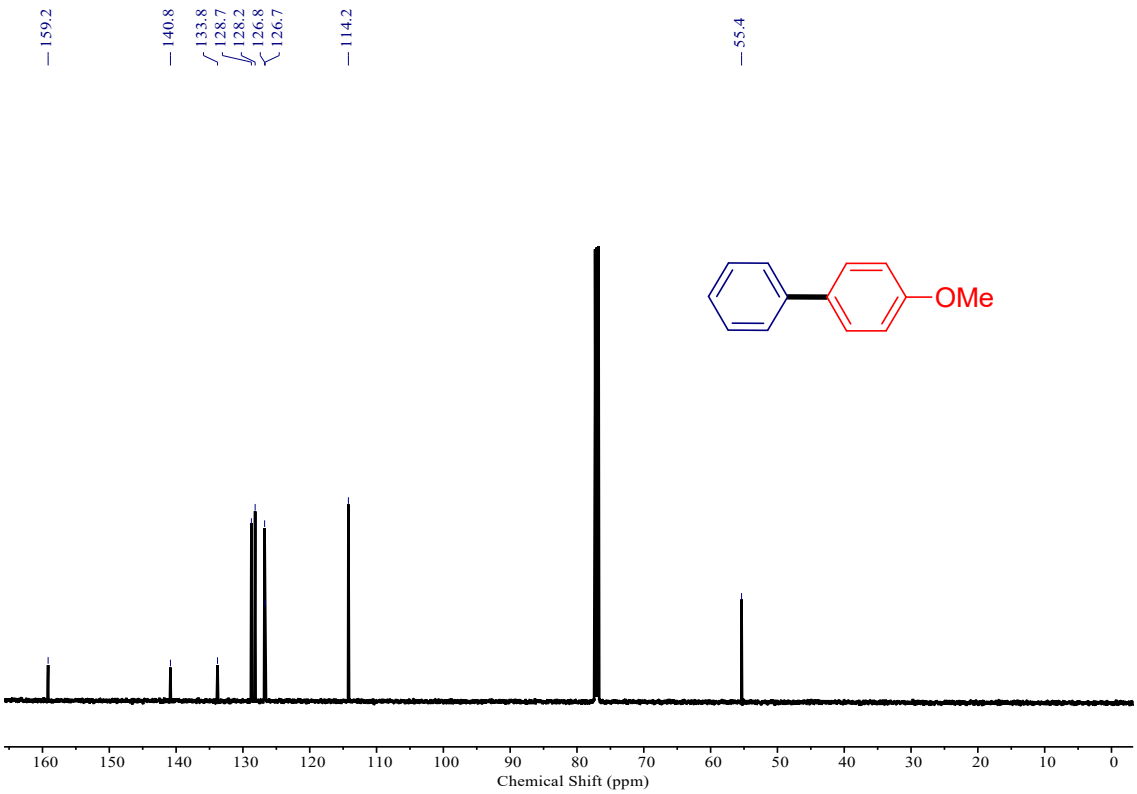

Fig. S12. ^{13}C NMR (125 MHz, $CDCl_3$) spectrum of 4-methoxy-1,1'-biphenyl **(3a)**.

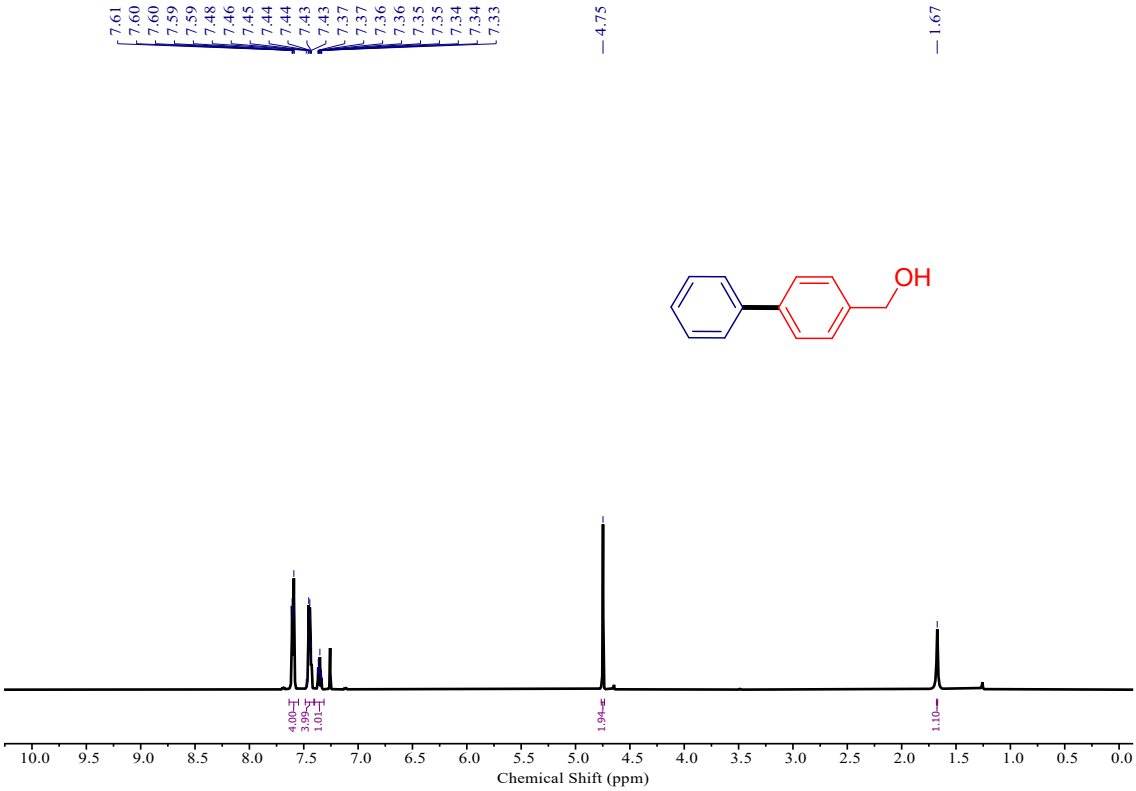

Fig. S13. ^{1}H NMR (500 MHz, $CDCl_3$) spectrum of [1,1'-biphenyl]-4-ylmethanol **(3b)**.

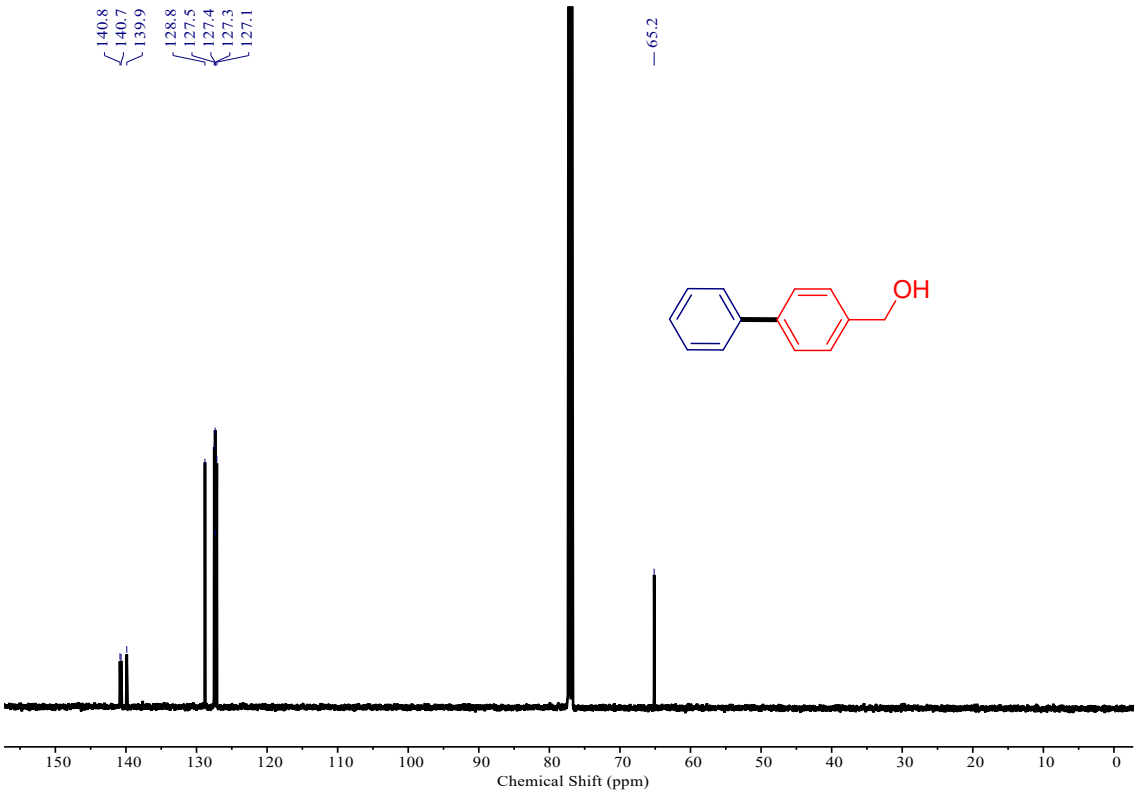

Fig. S14. ^{13}C NMR (125 MHz, $CDCl_3$) spectrum of [1,1'-biphenyl]-4-ylmethanol **(3b).**

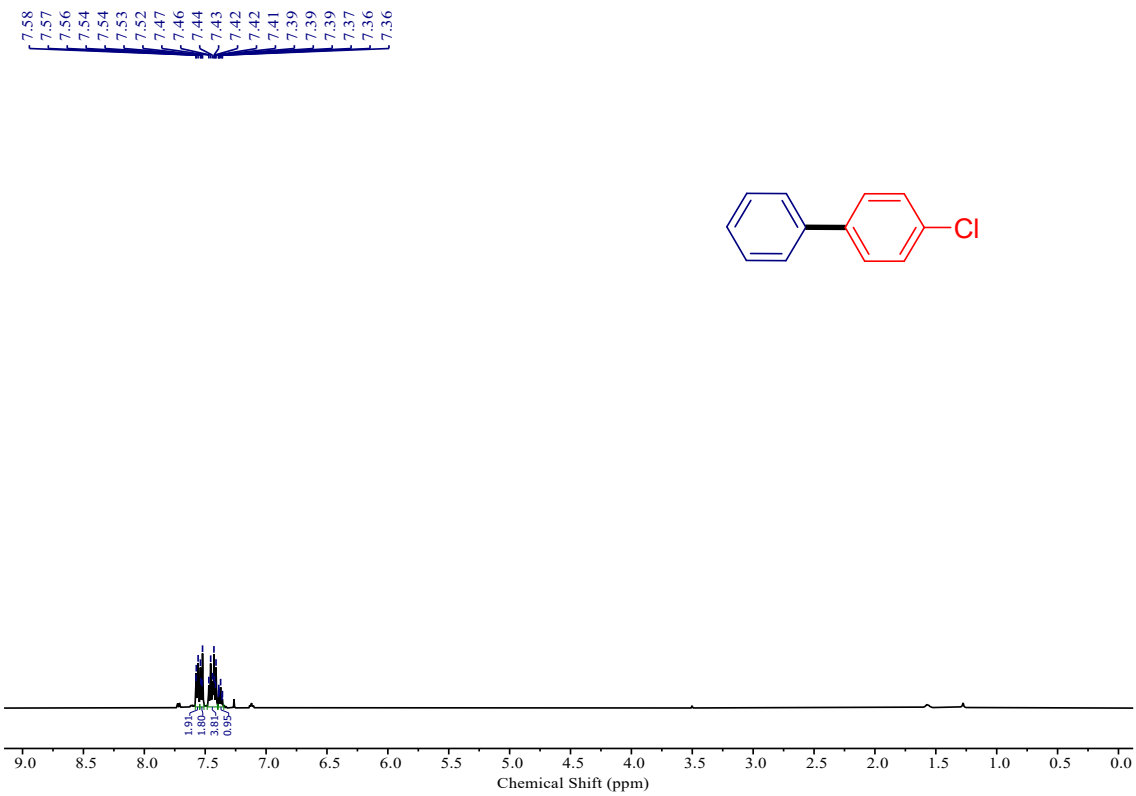

Fig. S15. ^{1}H NMR (500 MHz, $CDCl_3$) spectrum of 4-chloro-1,1'-biphenyl **(3c)**.

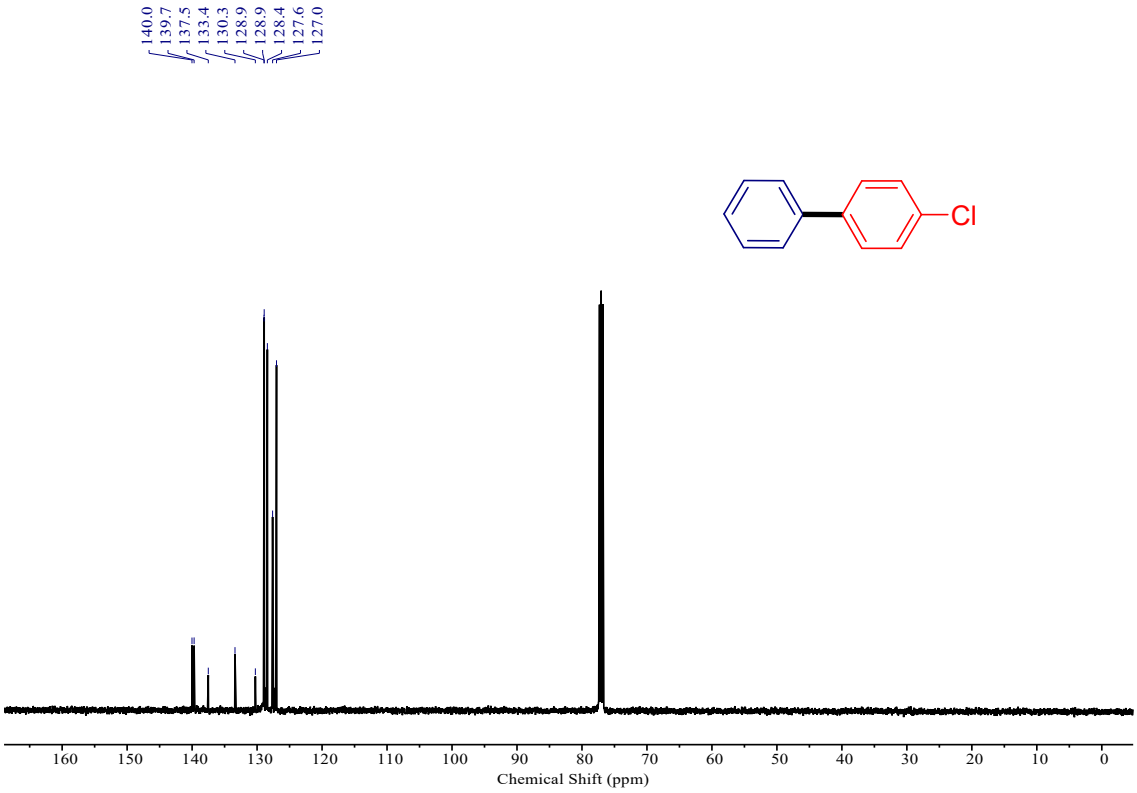

Fig. S16. ^{13}C NMR (125 MHz, $CDCl_3$) spectrum of 4-chloro-1,1'-biphenyl **(3c)**.

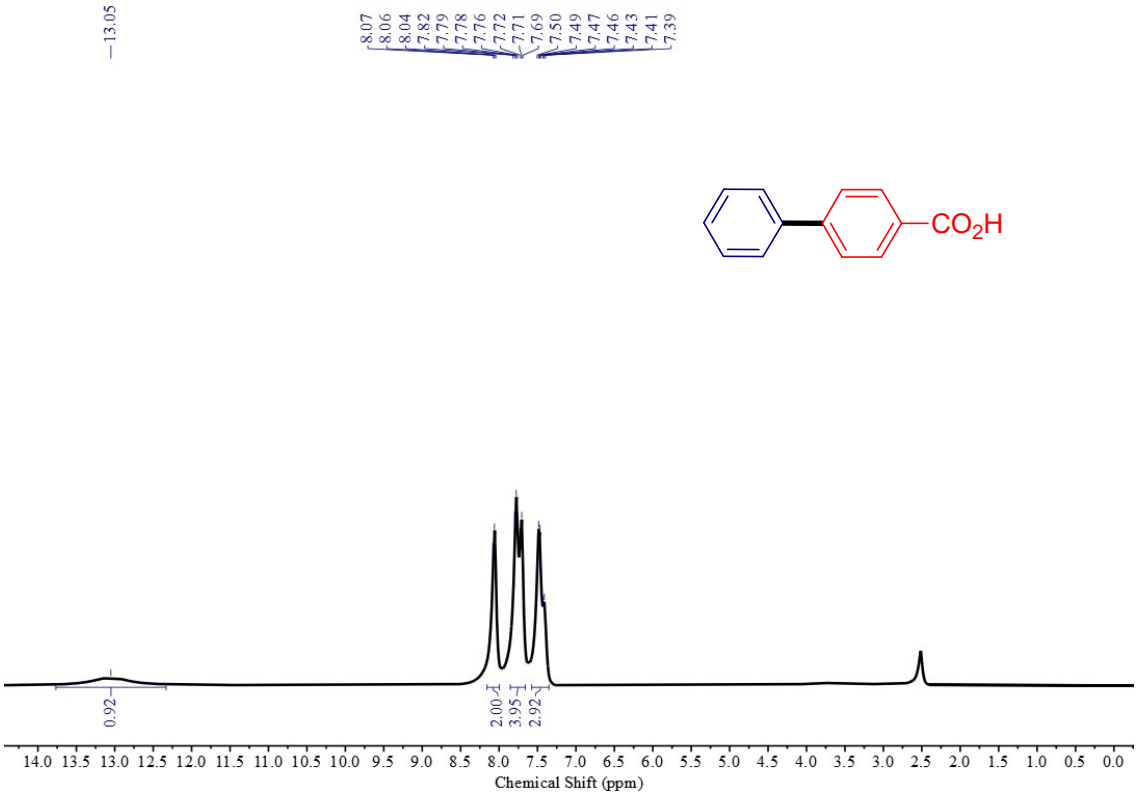

Fig. S17. ^{1}H NMR (500 MHz, DMSO-d_6) spectrum of [1,1'-biphenyl]-4-carboxylic acid **(3d)**.

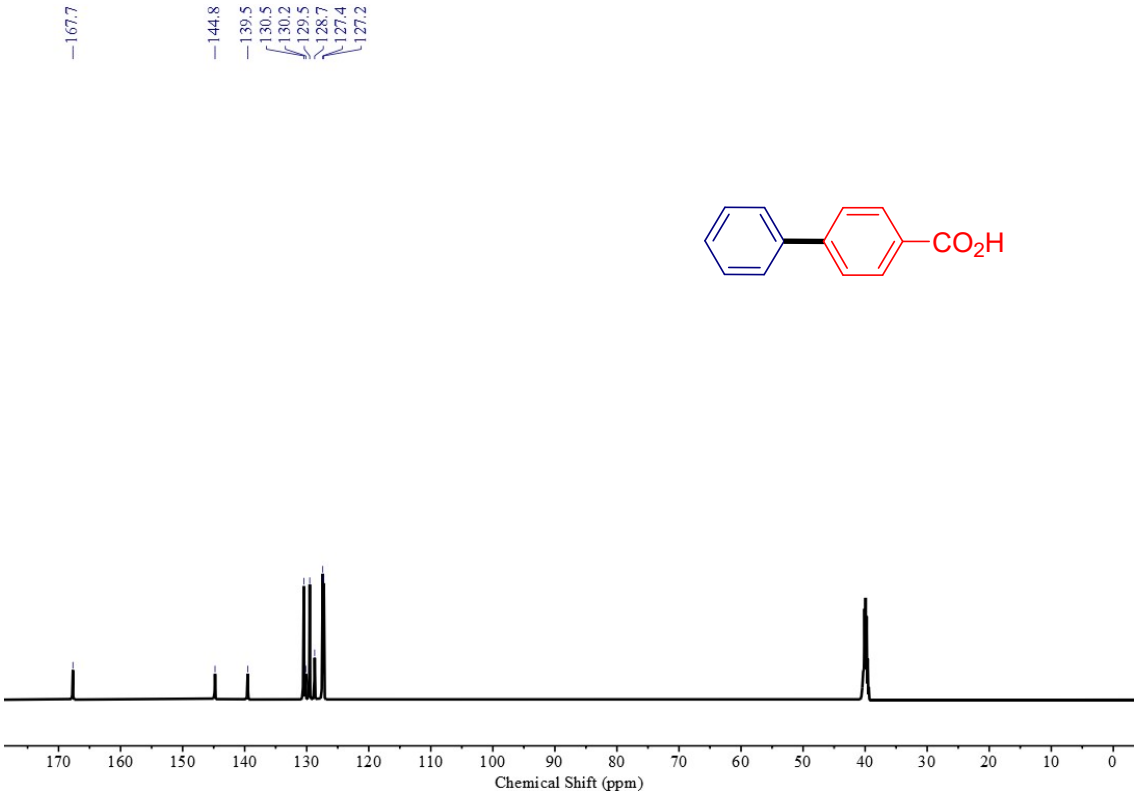

Fig. S18. ^{13}C NMR (125 MHz, DMSO-d_6) spectrum of [1,1'-biphenyl]-4-carboxylic acid **(3d)**.

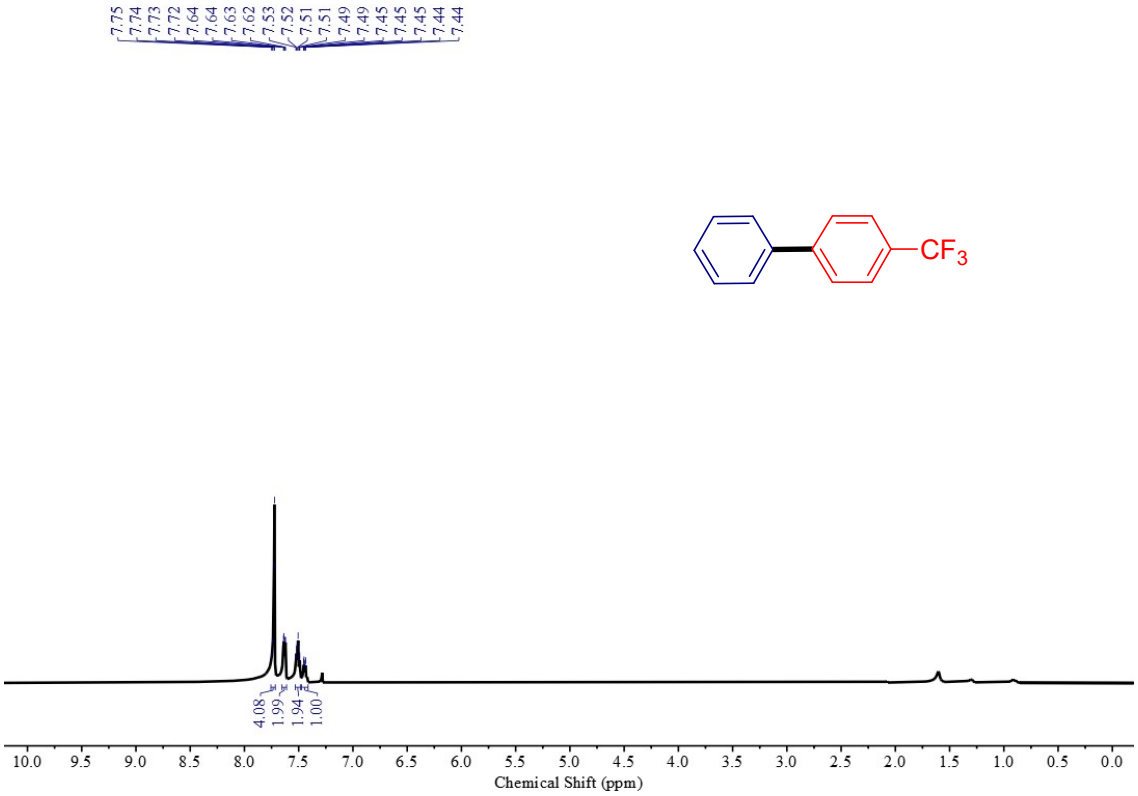

Fig. S19. ^{1}H NMR (500 MHz, $CDCl_3$) spectrum of 4-(trifluoromethyl)-1,1'-biphenyl **(3e)**.

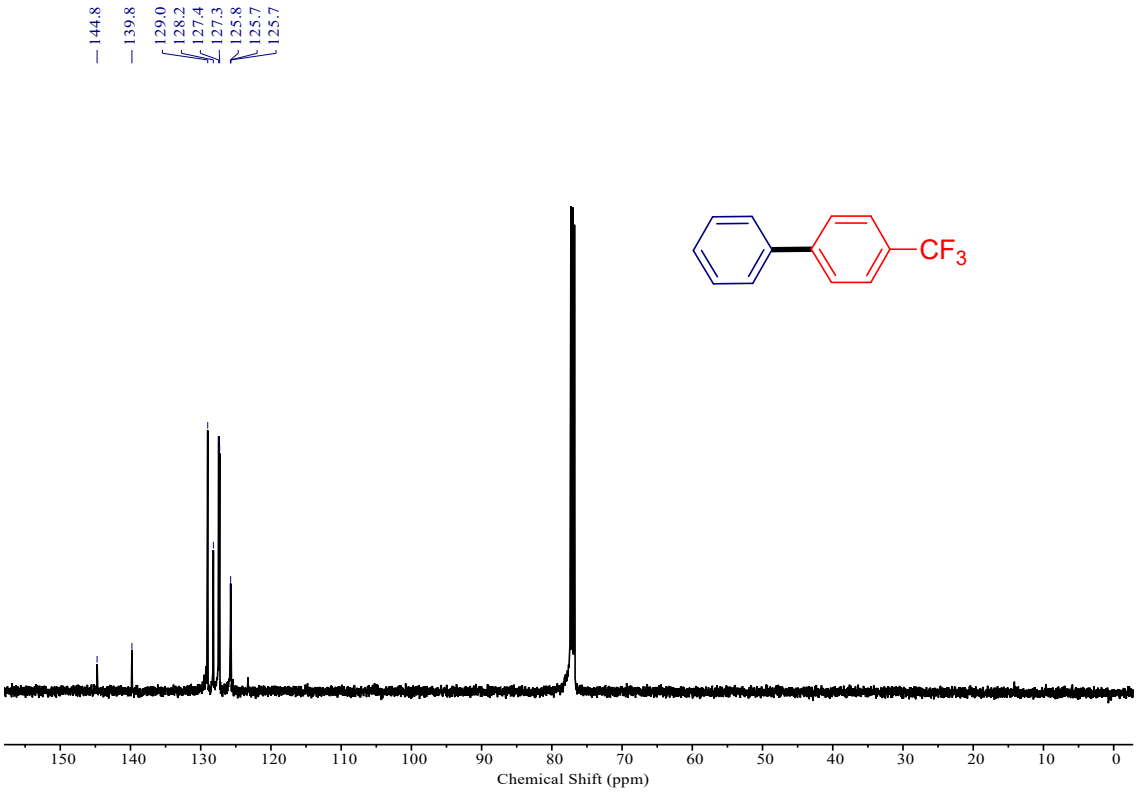

Fig. S20. ^{13}C NMR (125 MHz, $CDCl_3$) spectrum of 4-(trifluoromethyl)-1,1'-biphenyl **(3e)**.

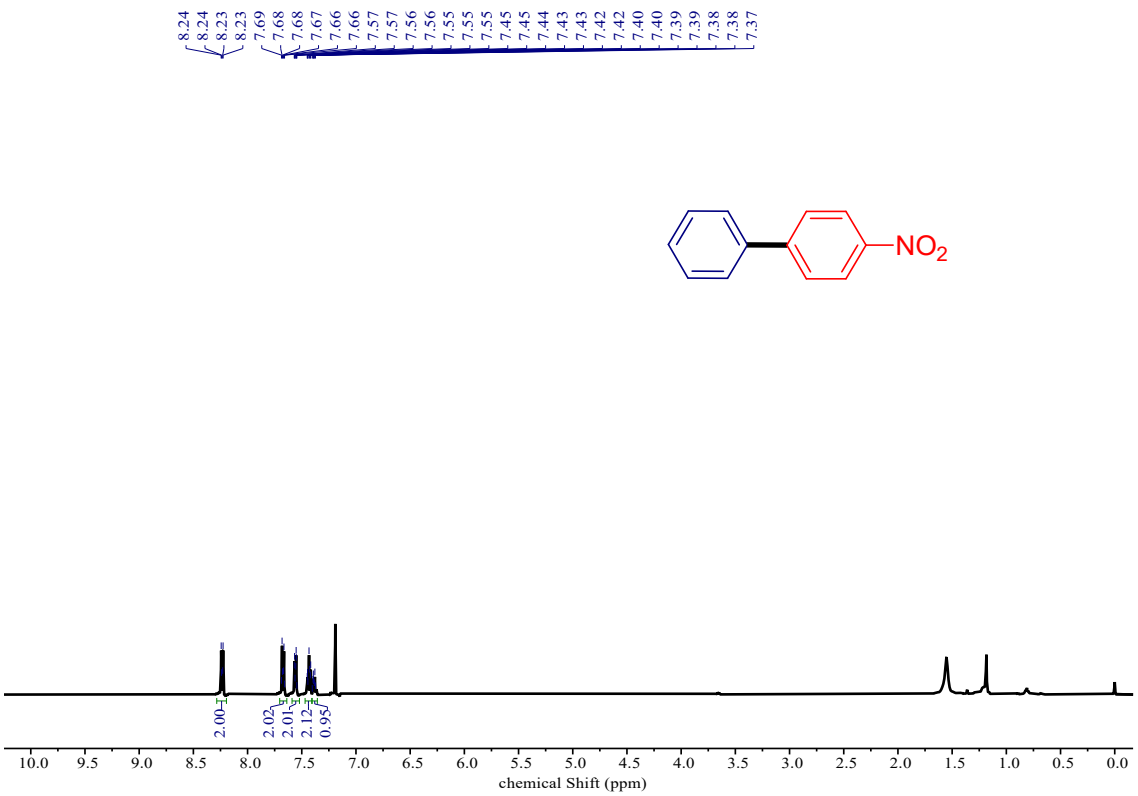

Fig. S21. ^{1}H NMR (500 MHz, $CDCl_3$) spectrum of 4-nitro-1,1'-biphenyl **(3f)**.

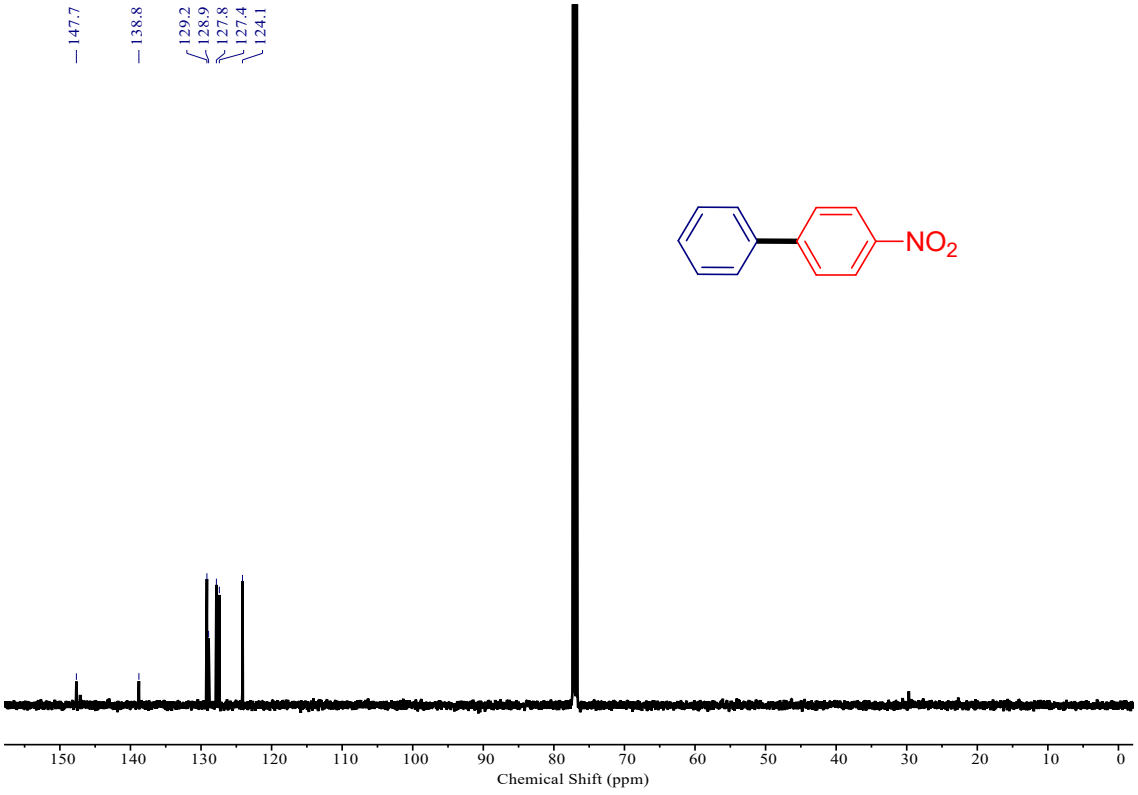

Fig. S22. ^{13}C NMR (125 MHz, $CDCl_3$) spectrum of 4-nitro-1,1'-biphenyl **(3f)**.

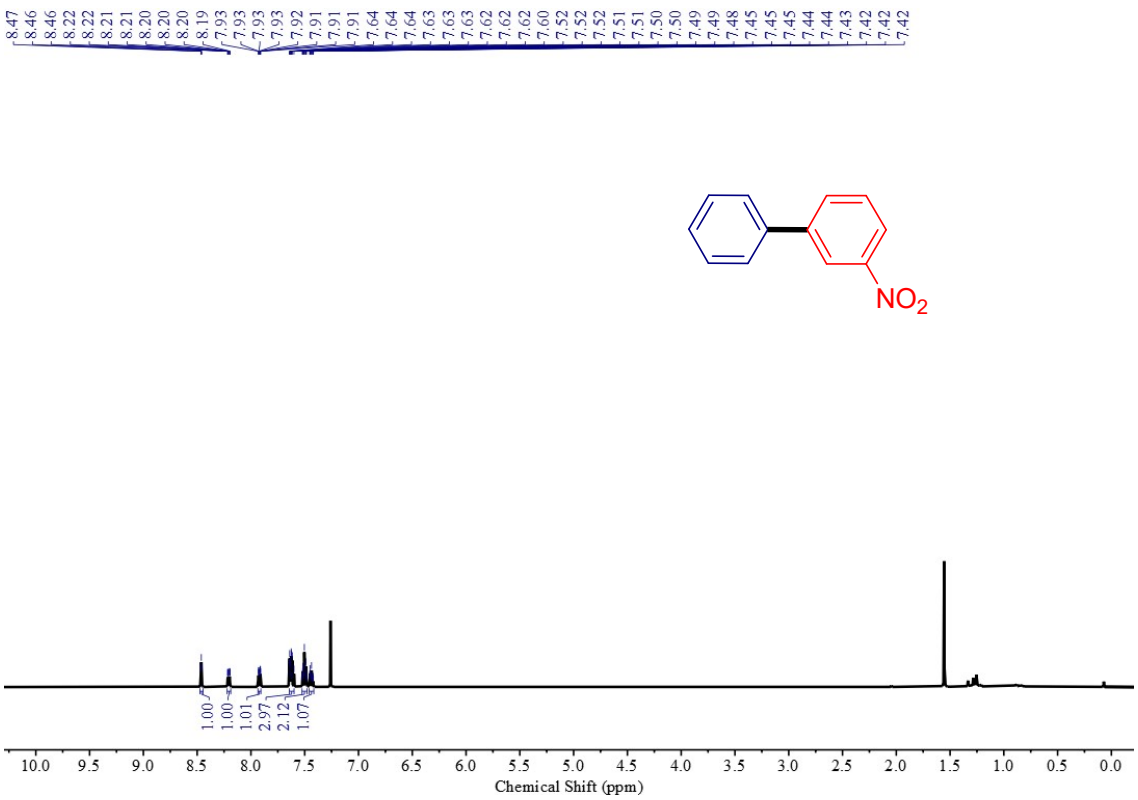

Fig. S23. ^{1}H NMR (500 MHz, $CDCl_3$) spectrum of 3-nitro-1,1'-biphenyl **(3g)**.

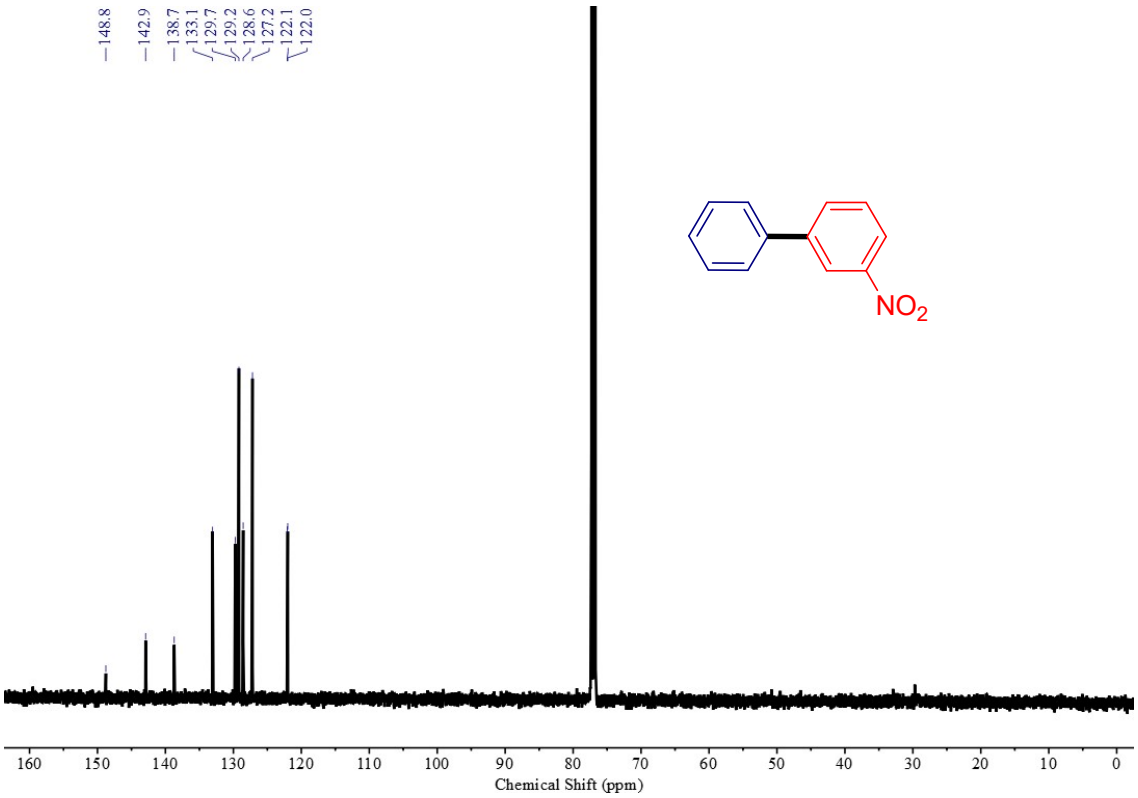

Fig. S24. ^{13}C NMR (125 MHz, $CDCl_3$) spectrum of 3-nitro-1,1'-biphenyl **(3g)**.

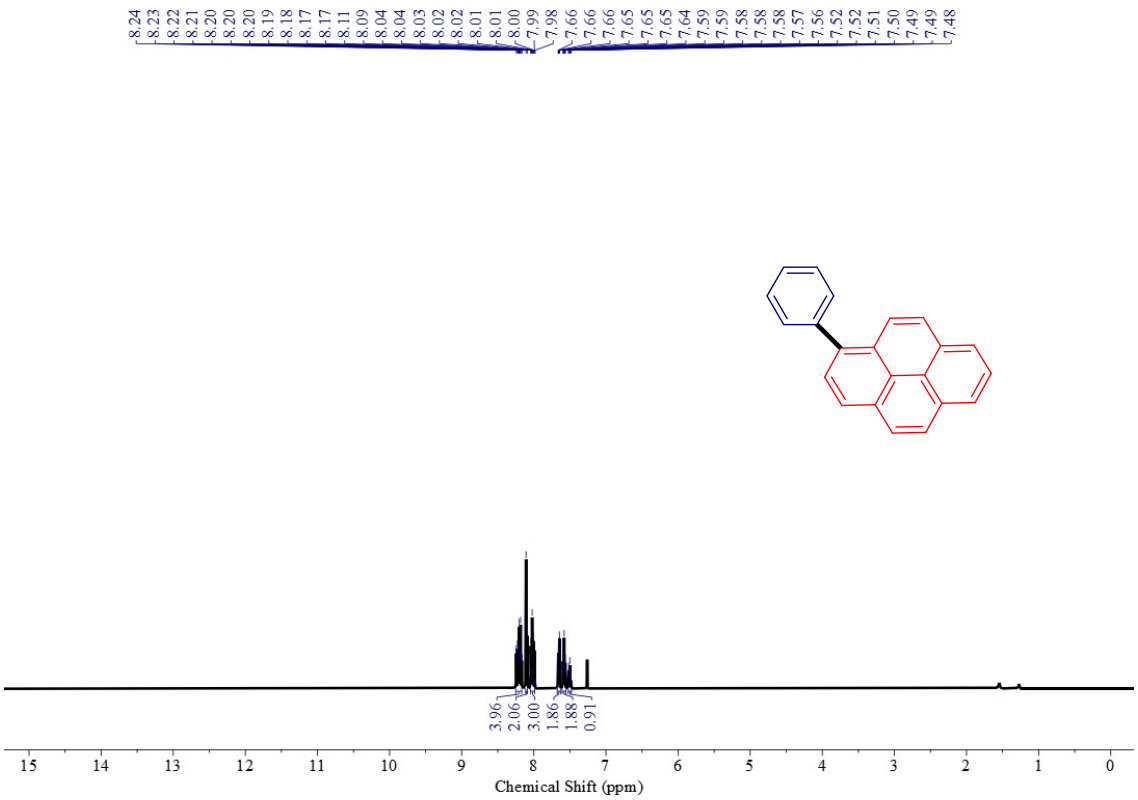

Fig. S25. ^{1}H NMR (500 MHz, $CDCl_3$) spectrum of 1-phenylpyrene **(3h)**.

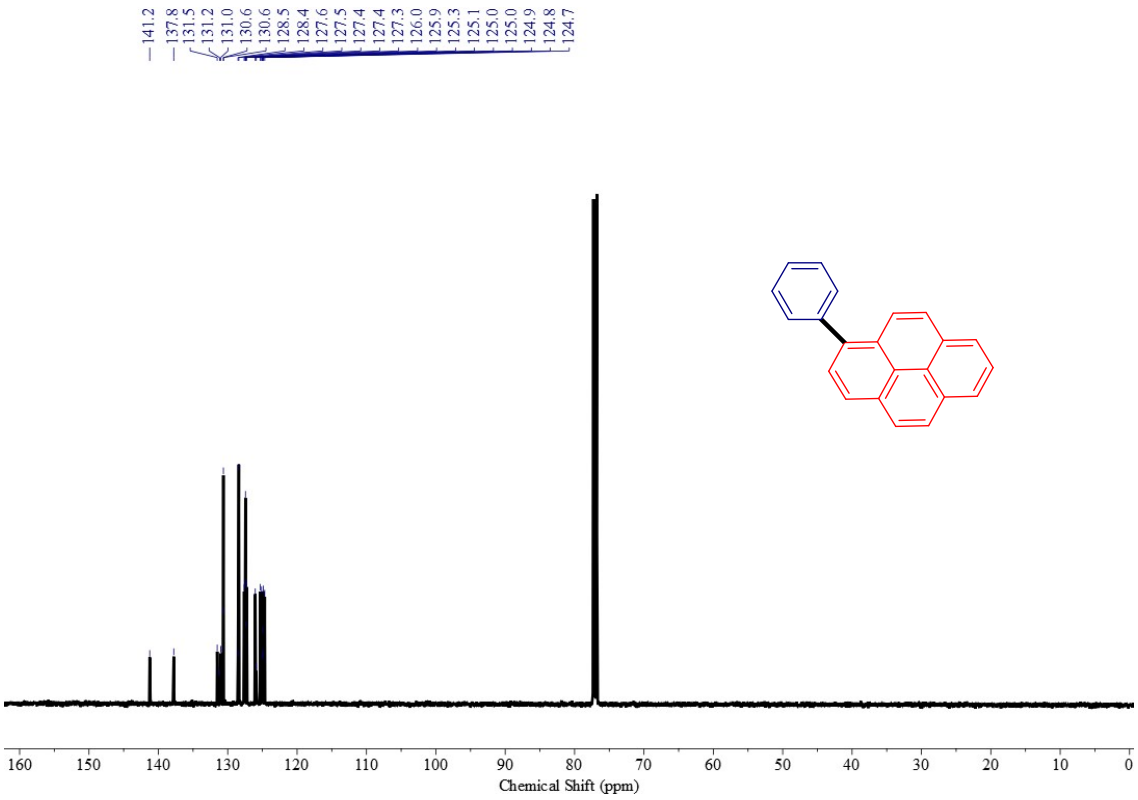

Fig. S26. ^{13}C NMR (125 MHz, $CDCl_3$) spectrum of 1-phenylpyrene **(3h)**.

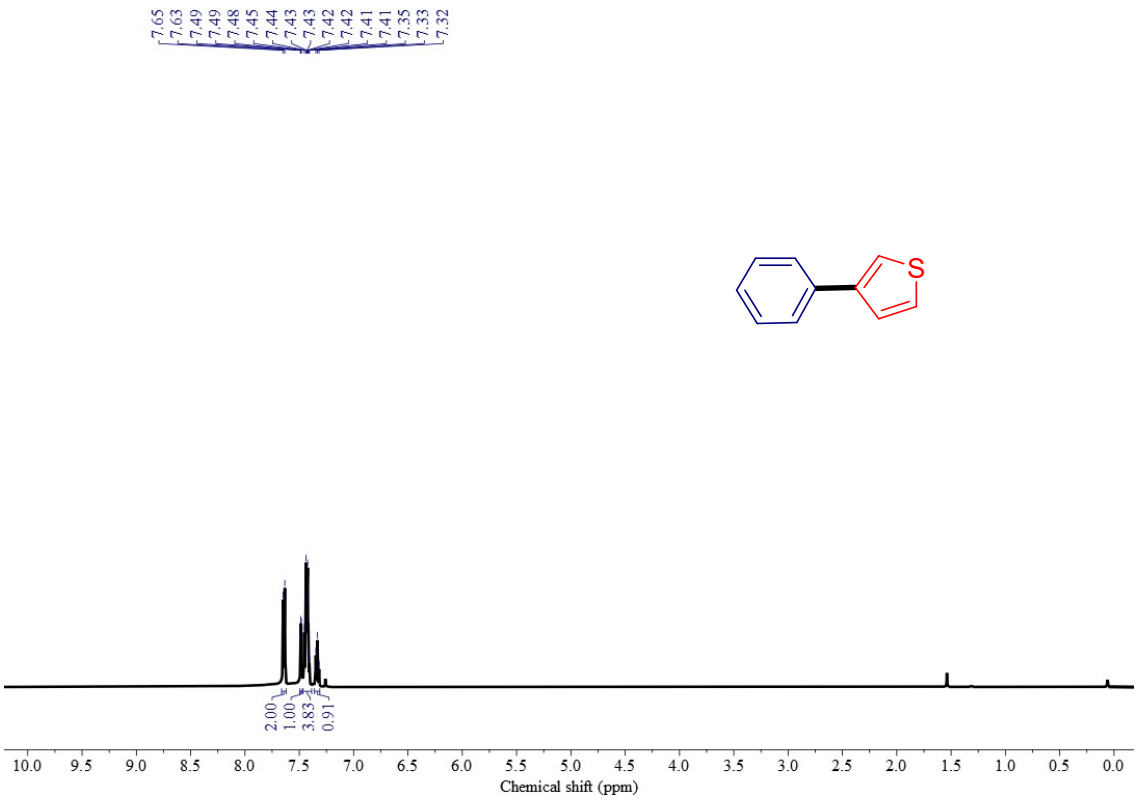

Fig. S27. ^{1}H NMR (500 MHz, $CDCl_3$) spectrum of 3-phenylthiophene **(3i)**

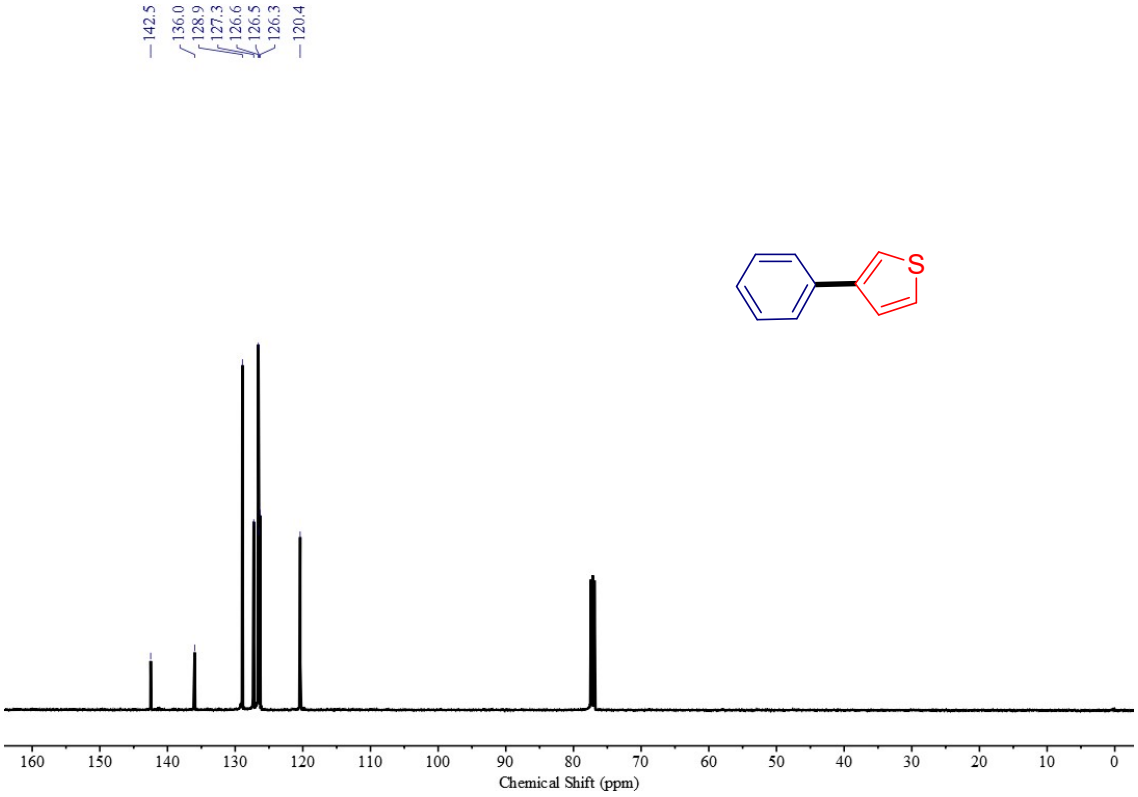

Fig. S28. ^{13}C NMR (125 MHz, $CDCl_3$) spectrum of 3-phenylthiophene **(3i)**.

^{1}H NMR and ^{13}C NMR data of all synthesised compounds

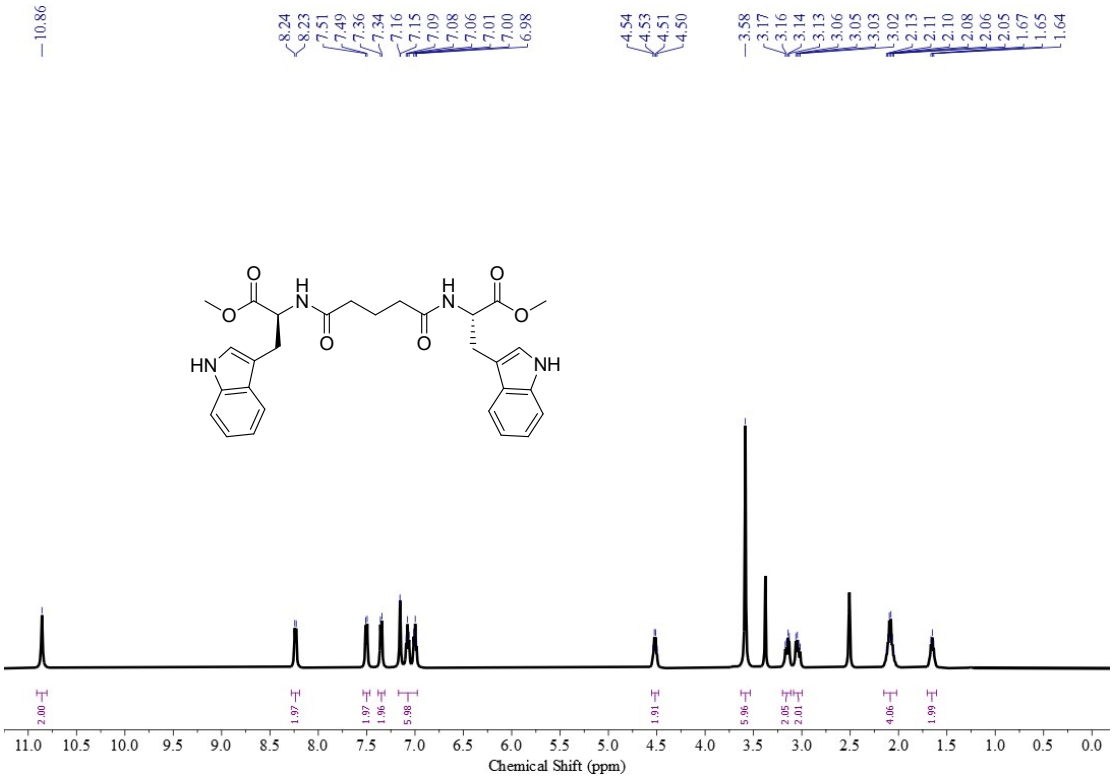

Fig. S29. ^{1}H NMR (500 MHz, DMSO-$d_{6,}$) spectrum of MeO-W-GluA-W-OMe **(4)**.

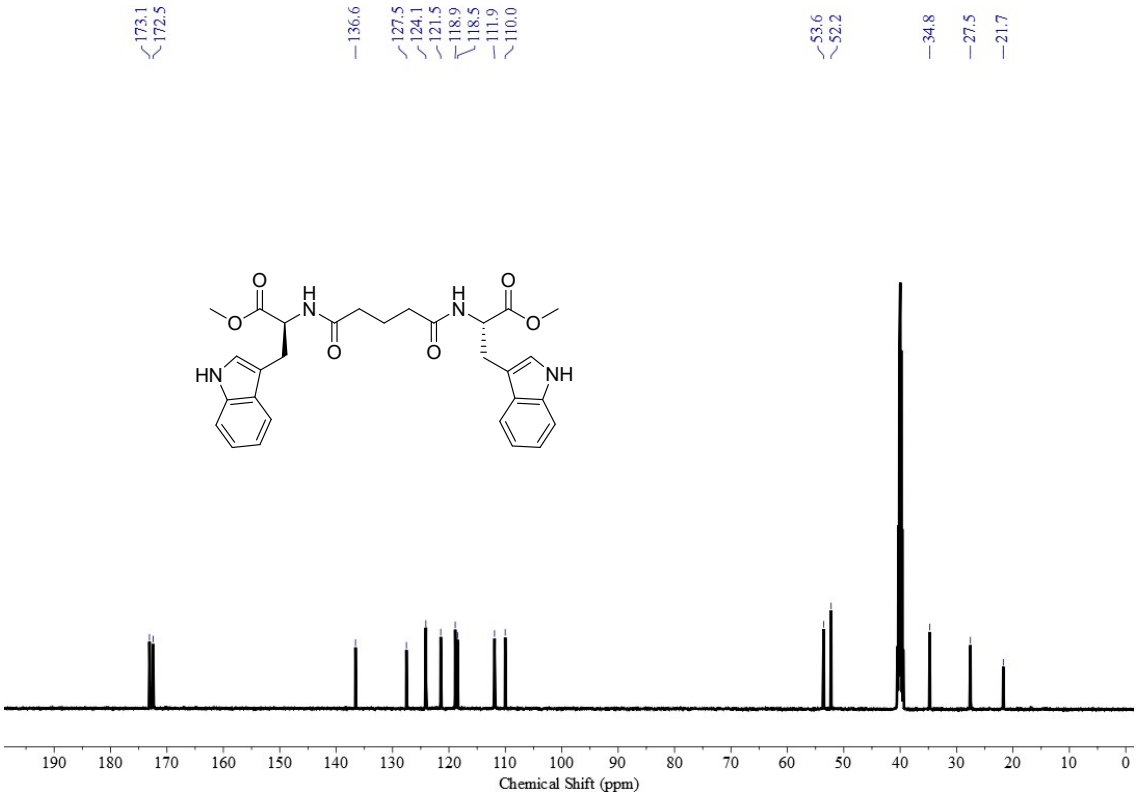

Fig. S30. ^{13}C NMR (125 MHz, DMSO-d_6) spectrum of MeO-W-GluA-W-OMe **(4)**.

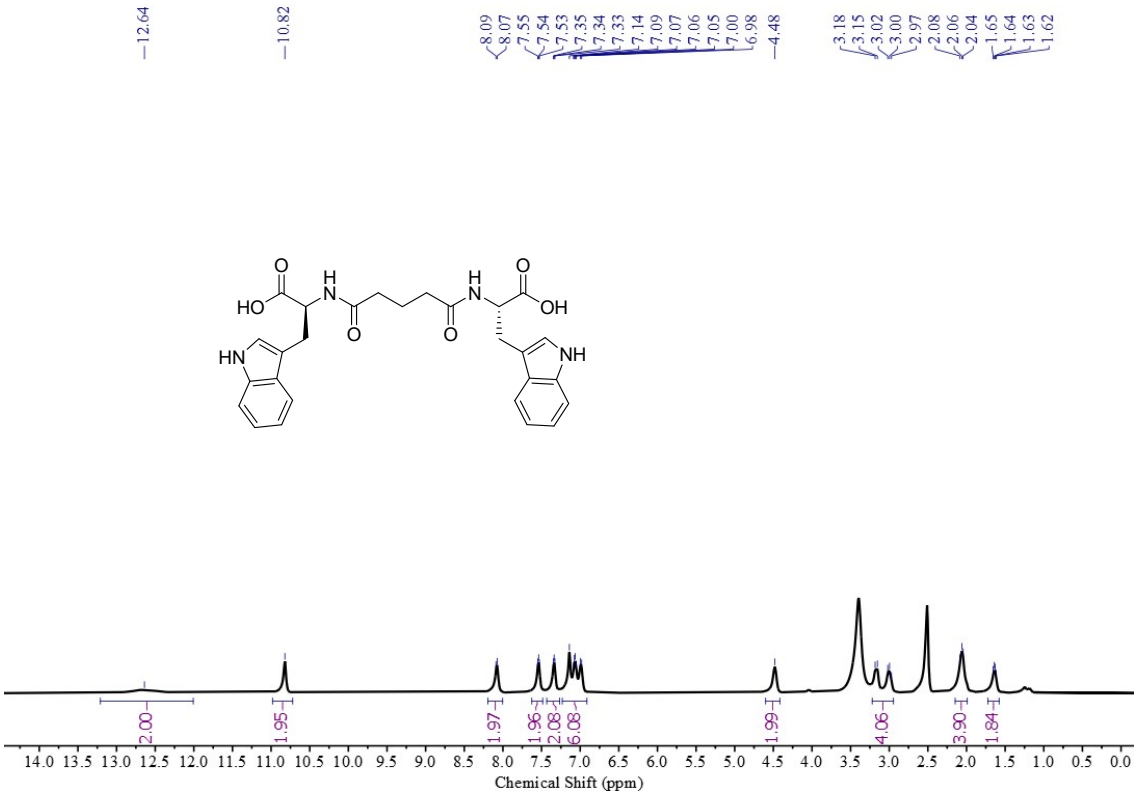

Fig. S31. ^{1}H NMR (500 MHz, DMSO-d_6) spectrum of HO-W-GluA-W-OH **(5)**.

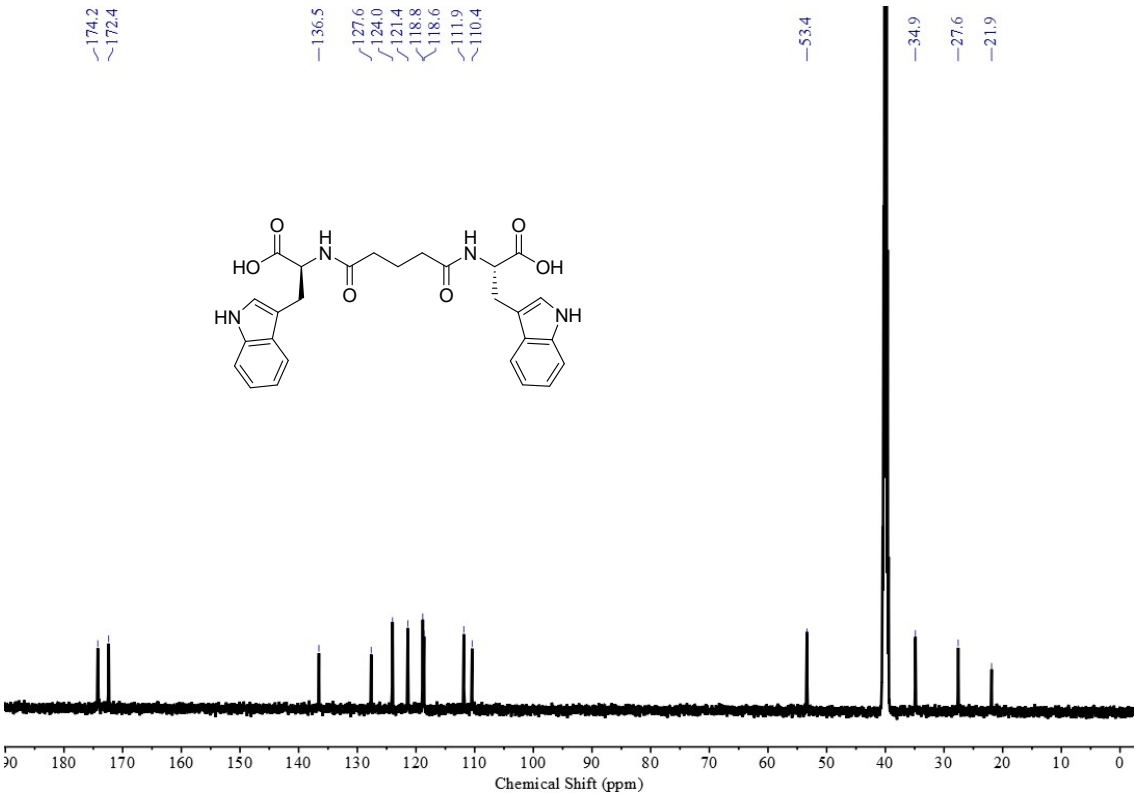

Fig. S32. ^{13}C NMR (125 MHz, DMSO-d_6) spectrum of HO-W-GluA-W-OH **(5)**.

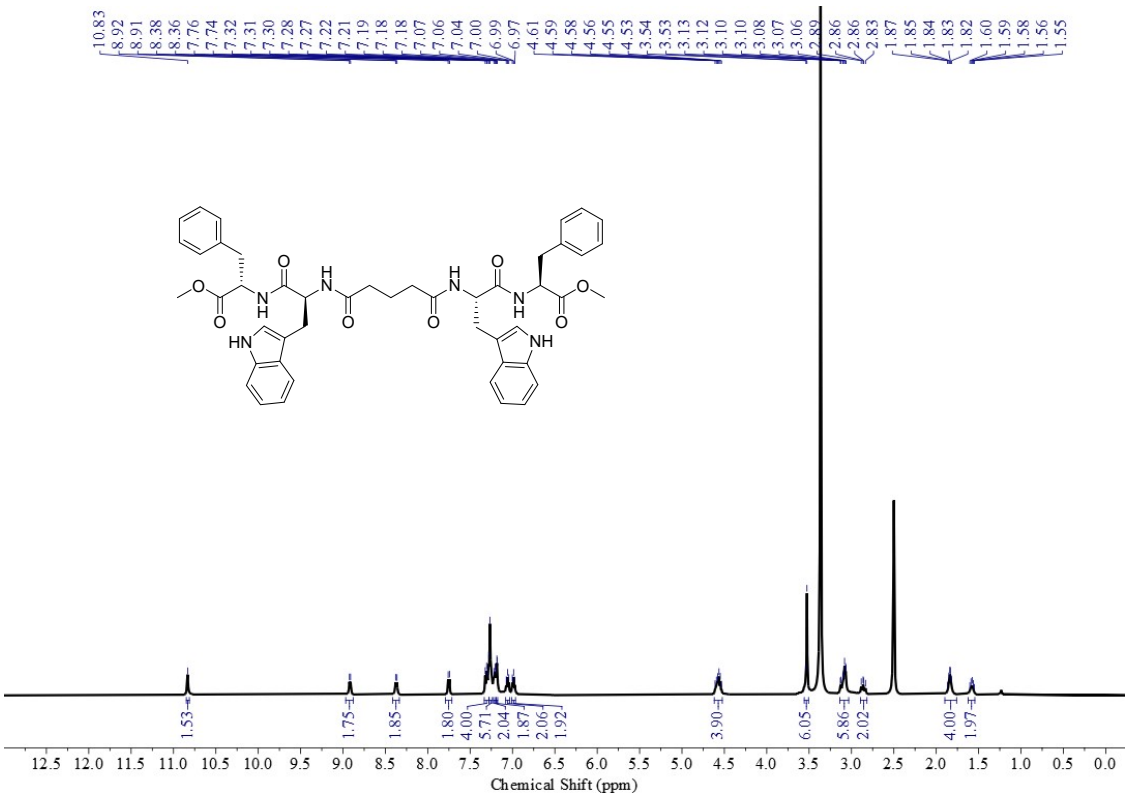

Fig. S33. ^{1}H NMR (500 MHz, DMSO-d_6) spectrum of MeO-F-W-GluA-W-F-OMe **(7)**.

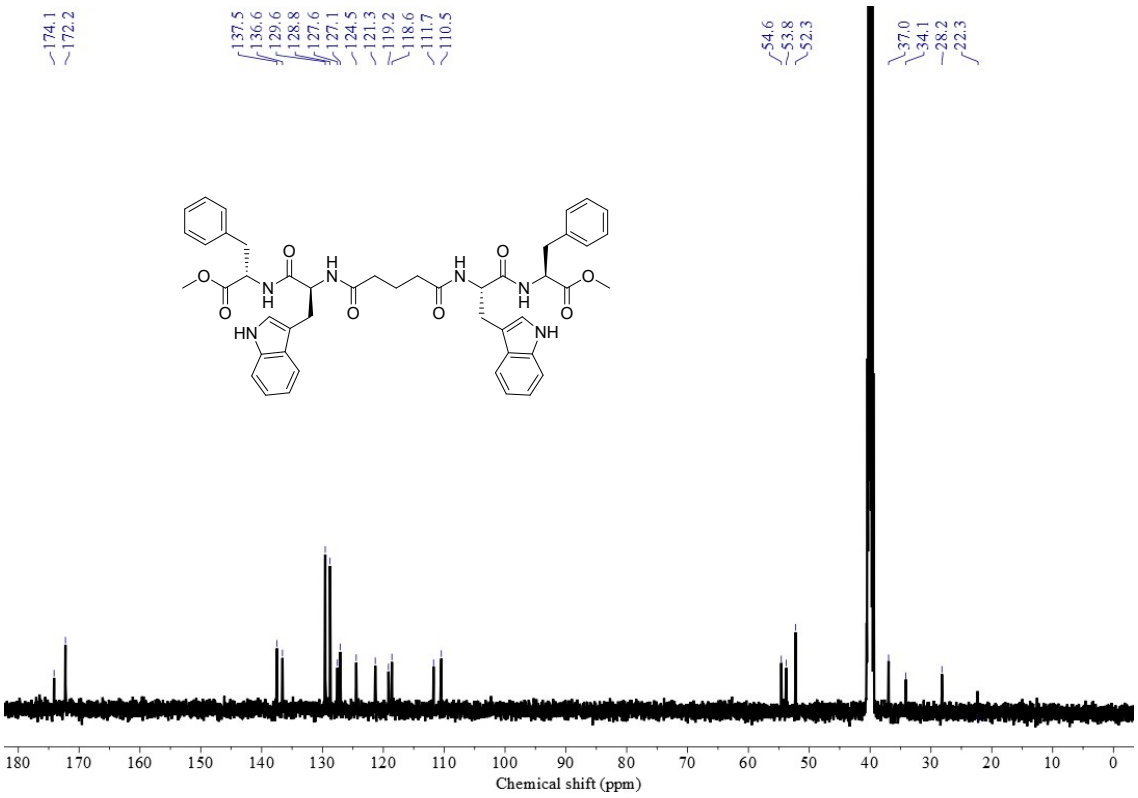

Fig. S34. ^{13}C NMR (125 MHz, DMSO-d_6) spectrum of MeO-F-W-GluA-W-F-OMe **(7)**.

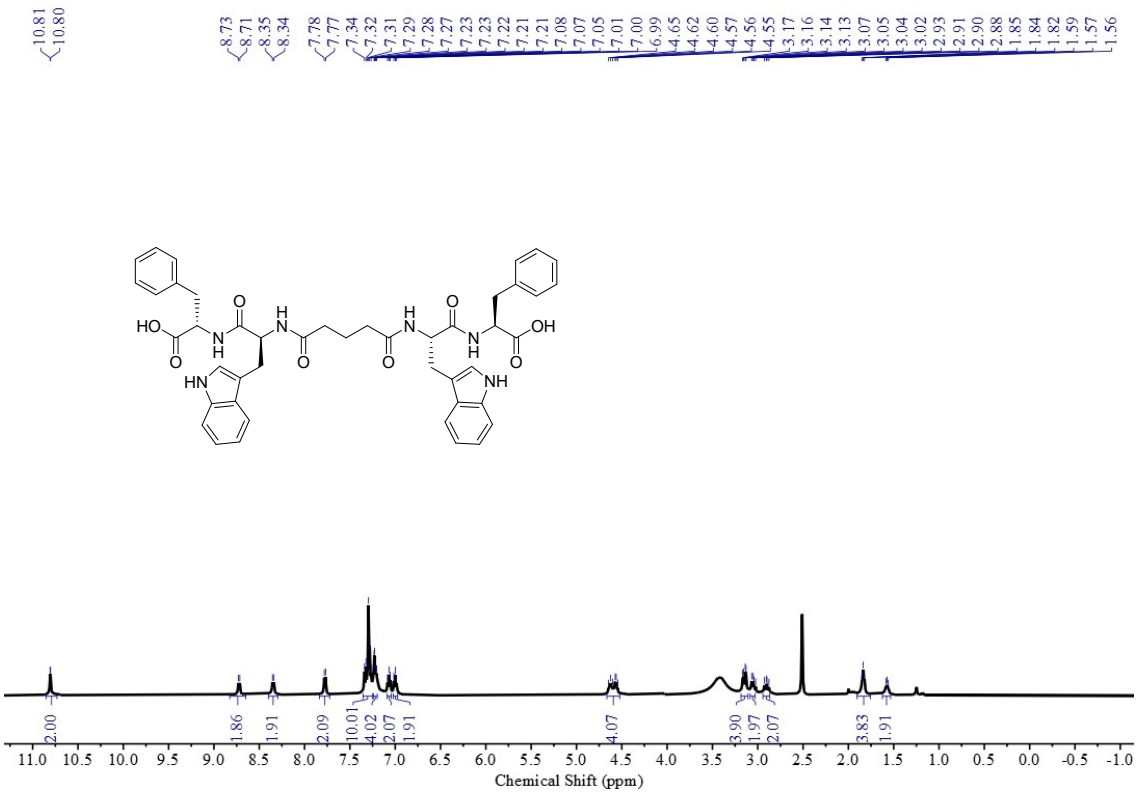

Fig. S35. ^{1}H NMR (, 500 MHz, DMSO-d_6) spectrum of HO-F-W-GluA-W-F-OH **(1)**.

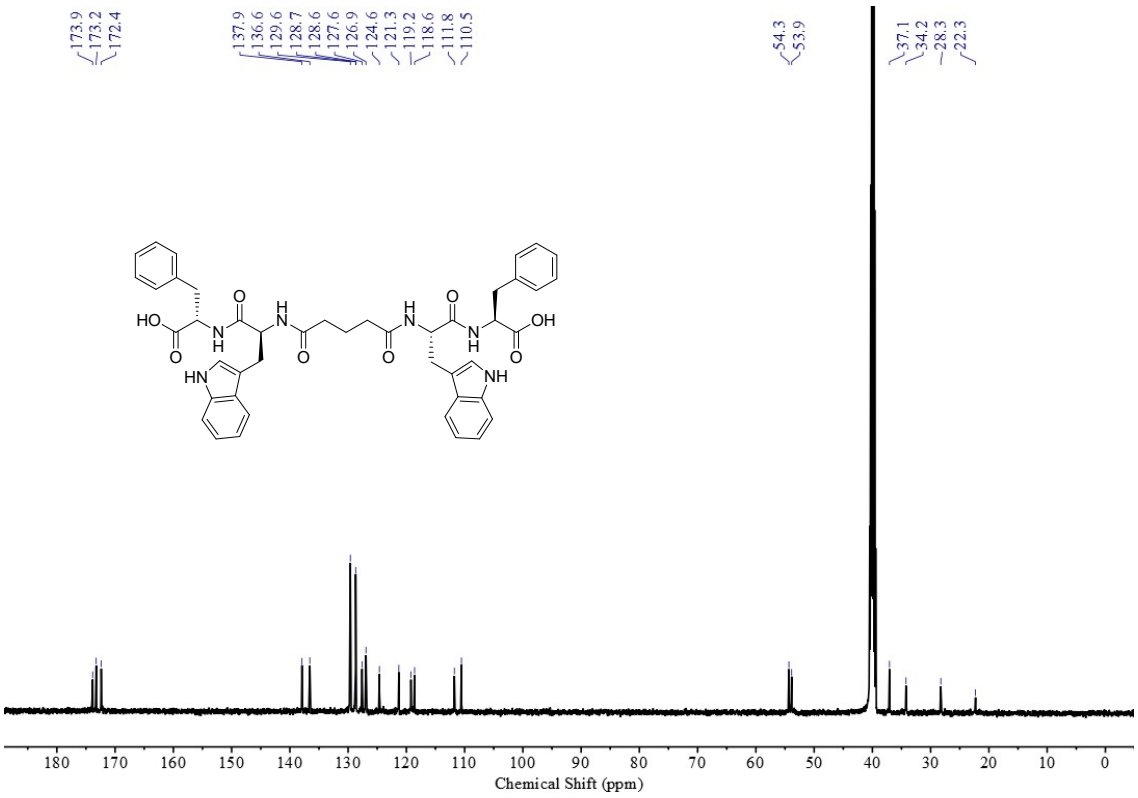

Fig. S36. ^{13}C NMR (125 MHz, DMSO-d_6) spectrum of HO-F-W-GluA-W-F-OH **(1)**.

Mass spectrometry data of all synthesised compounds

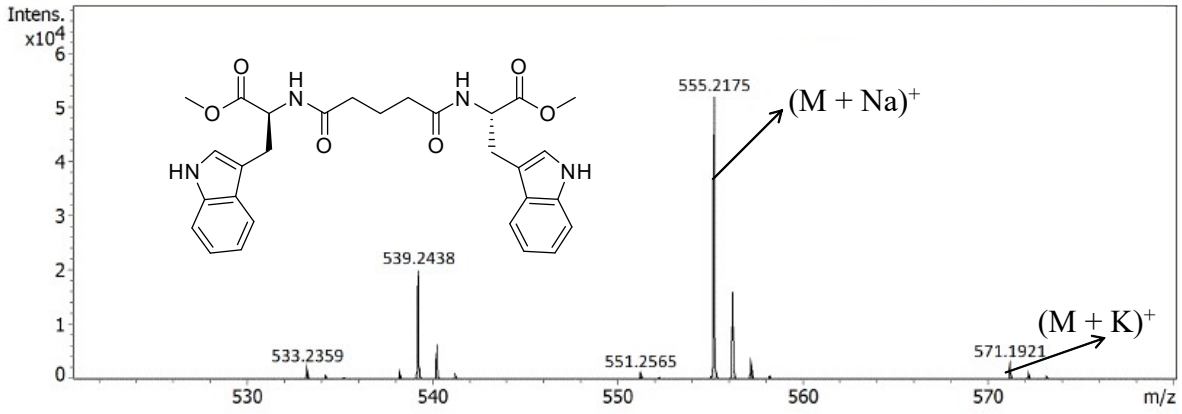

Fig. S37. ESI-MS spectrum of MeO-W-GluA-W-OMe **(4)**.

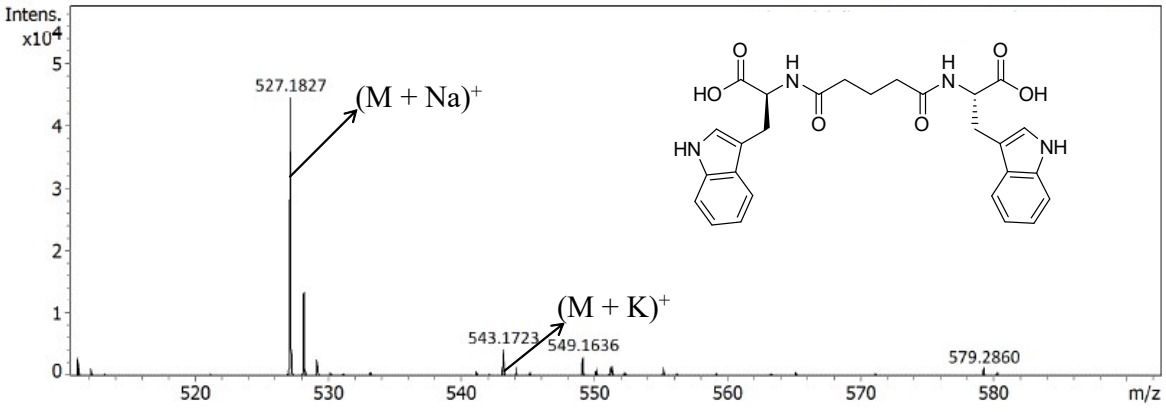

Fig. S38. ESI-MS spectrum of HO-W-GluA-W-OH **(5)**.

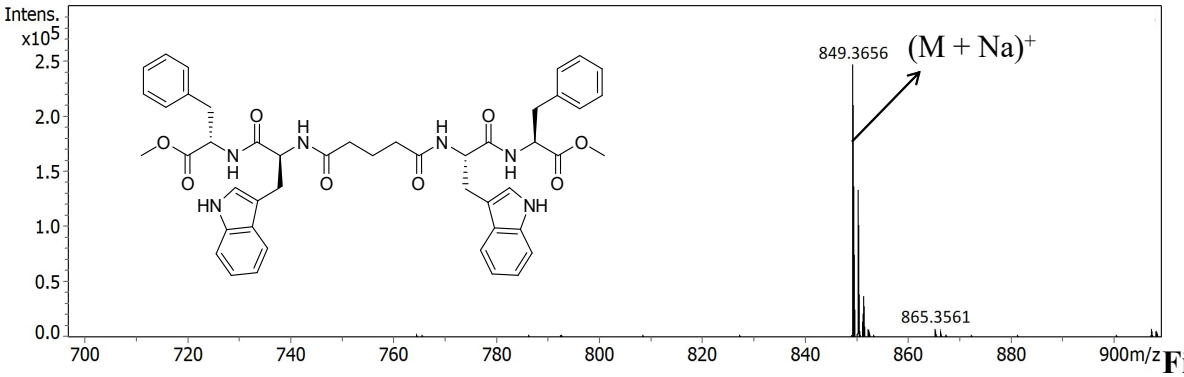

Fig. S39. ESI-MS spectrum of MeO-F-W-GluA-W-F-OMe **(7)**.

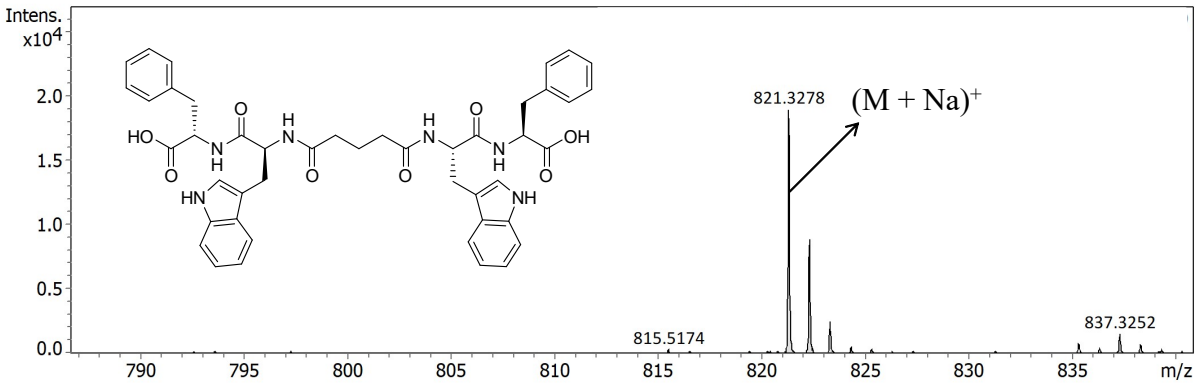

Fig. S40. ESI-MS spectrum of HO-F-W-GluA-W-F-OH **(1)**.